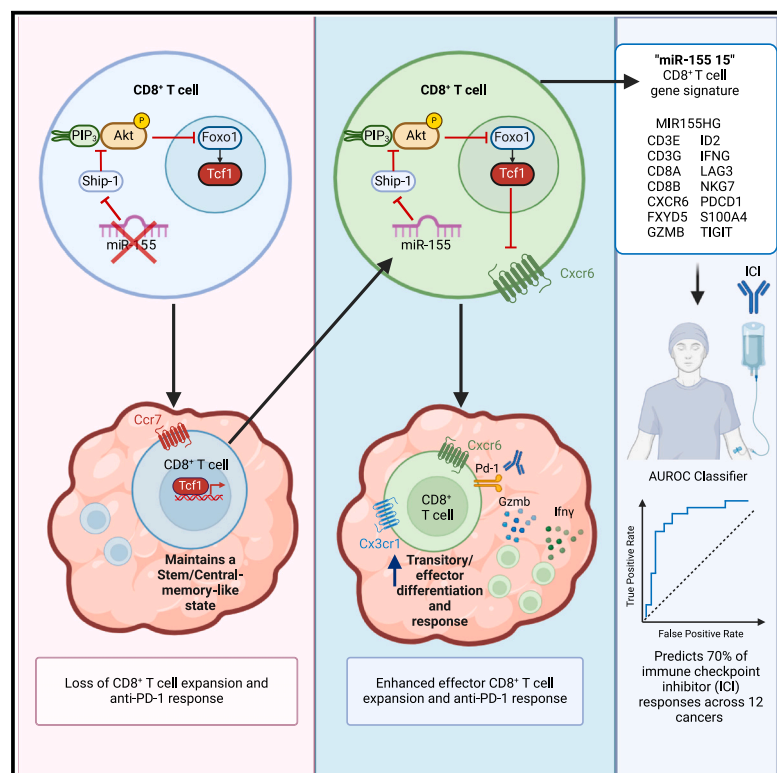


A microRNA-regulated transcriptional state defines intratumoral CD8⁺ T cells that respond to immunotherapy

Graphical abstract



Authors

William W. Tang, Ben Battistone, Kaylyn M. Bauer, ..., H. Atakan Ekiz, Warren P. Voth, Ryan M. O'Connell

Correspondence

ryan.oconnell@path.utah.edu

In brief

Tang et al. describe a critical molecule, miR-155, which enhances CD8⁺ T cells that combat CRC and respond to immunotherapy. In multiple human cancers, miR-155 defines a CD8⁺ T cell state that predicts immunotherapy responses and may serve as a biomarker of immunotherapy candidates, potentially enhancing therapeutic and patient outcomes.

Highlights

- miR-155 is necessary for intratumor effector Cxcr6⁺CD8⁺ T cell differentiation
- Tumor immunity and ICI require miR-155 expression in tumor-targeting CD8⁺ T cells
- Ship-1 and, subsequently, Foxo1 and Tcf-1 are inhibited by miR-155, allowing CXCR6 expression
- A miR-155-dependent CD8⁺ T cell gene signature predicts pan-cancer ICI responses



Article

A microRNA-regulated transcriptional state defines intratumoral CD8⁺ T cells that respond to immunotherapy

William W. Tang,^{1,7} Ben Battistone,^{1,7} Kaylyn M. Bauer,^{1,7} Allison M. Weis,^{1,7} Cindy Barba,^{1,7} Muhammad Zaki Hidayatullah Fadlullah,^{3,7} Arevik Ghazaryan,^{1,7} Van B. Tran,^{1,7} Soh-Hyun Lee,^{1,7} Z. Busra Agir,⁴ Morgan C. Nelson,^{1,7} Emmanuel Stephen Victor,^{1,7} Amber Thibeaux,^{1,7} Colton Hernandez,^{1,7} Jacob Tantalla,^{1,7} Aik C. Tan,^{3,7} Dinesh Rao,⁶ Matthew Williams,^{1,7} Micah J. Drummond,² Ellen J. Beswick,⁵ June L. Round,^{1,7} H. Atakan Ekiz,^{1,4,7} Warren P. Voth,^{1,7} and Ryan M. O'Connell^{1,6,8,*}

¹Department of Pathology, Division of Microbiology and Immunology, University of Utah, Salt Lake City, UT 84112, USA

²Department of Physical Therapy and Athletic Training, University of Utah, Salt Lake City, UT 84108, USA

³Department of Oncological Sciences, University of Utah, Salt Lake City, UT 84112, USA

⁴Department of Molecular Biology and Genetics, İzmir Institute of Technology, İzmir, Turkey

⁵Division of Digestive Disease and Nutrition, Department of Internal Medicine, University of Kentucky, Lexington, KY 40508, USA

⁶Department of Pathology and Laboratory Medicine, University of California, Los Angeles, Los Angeles, CA 90095, USA

⁷Huntsman Cancer Institute, University of Utah, Salt Lake City, UT 84112, USA

⁸Lead contact

*Correspondence: ryan.oconnell@path.utah.edu

<https://doi.org/10.1016/j.celrep.2025.115301>

SUMMARY

The rising incidence of advanced-stage colorectal cancer (CRC) and poor survival outcomes necessitate new and effective therapies. Immune checkpoint inhibitors (ICIs), specifically anti-PD-1 therapy, show promise, yet clinical determinants of a positive response are suboptimal. Here, we identify microRNA-155 (miR-155) as necessary for CD8⁺ T cell-infiltrated tumors through an unbiased *in vivo* CRISPR-Cas9 screen identifying functional tumor antigen-specific CD8⁺ T cell-expressed microRNAs. T cell miR-155 is required for anti-PD-1 responses and for a vital intratumor CD8⁺ T cell differentiation cascade by repressing Ship-1, inhibiting Tcf-1 and stemness, and subsequently enhancing Cxcr6 expression, anti-tumor immunity, and effector functions. Based on an underlying miR-155-dependent CD8⁺ T cell transcriptional profile, we identify a gene signature that predicts ICI responses across 12 diverse cancers. Together, our findings support a model whereby miR-155 serves as a central regulator of CD8⁺ T cell-dependent cancer immunity and ICI responses that may be leveraged for future therapeutics.

INTRODUCTION

In the United States, colorectal cancer (CRC) is the third deadliest and most common cancer despite significant reductions in incidence and mortality due to improved screening.^{1,2} However, the incidence of metastatic CRC (mCRC) has been increasing in younger individuals³ and has a survival rate of just 14% with current treatments, necessitating new therapeutic options.^{3,4} Immune checkpoint inhibitors (ICIs) have drastically improved patient survival of many solid tumor types by inhibiting PD-1 and reinvigorating PD-1⁺ CD8⁺ T cells to resume their anti-tumor function.⁵ Pembrolizumab and nivolumab, two PD-1 inhibitors, induce robust T cell-mediated antitumor responses in mCRC with high microsatellite instability (MSI-H).^{6,7} MSI-H is often due to deficiency in mismatch repair (dMMR) enzymes, resulting in increased genetic instability, tumor mutational burden, and neoantigen load, which enhance T cell-mediated anti-tumor and ICI responses. Although dMMR/MSI-H status is the standard clinical predictor for ICI response, a large percentage of

dMMR/MSI-H patients do not respond to ICI.^{8–12} Additionally, dMMR/MSI-H patients represent a minority of patients with CRC,¹³ and ICI response rates are discordant with dMMR/MSI-H status as a consequence of tumor heterogeneity and T cell infiltration.¹⁴ Rather than utilizing tumor-intrinsic factors, the field has successfully used CD8⁺ T cell-dependent metrics as predictors of positive patient and therapy outcomes,^{15–18} making it clear that characterizing these metrics will be key determinants of ICI responses in CRC along with other cancers.

CD8⁺ T cells promote anti-tumor immunity and ICI responses through many states: stem like, transitory, and effector.^{19–26} The stem-like Tcf-1⁺ CD8⁺ T cells in tumors and tumor-draining lymph nodes (tdLNs) are a reservoir for expanding primed anti-tumor CD8⁺ T cells in the tumor microenvironment (TME).^{19,20,22,27,28} These stem-like CD8⁺ T cells enter a hyperproliferative Cx3cr1⁺ transitory state before becoming anti-tumor Cxcr6⁺CD8⁺ T cells.^{24,26,29,30} Cxcr6⁺ CD8⁺ T cells are highly specific to the effector state and TME, necessary for the expansion of an intratumoral CD8⁺ T cell niche required for anti-tumor



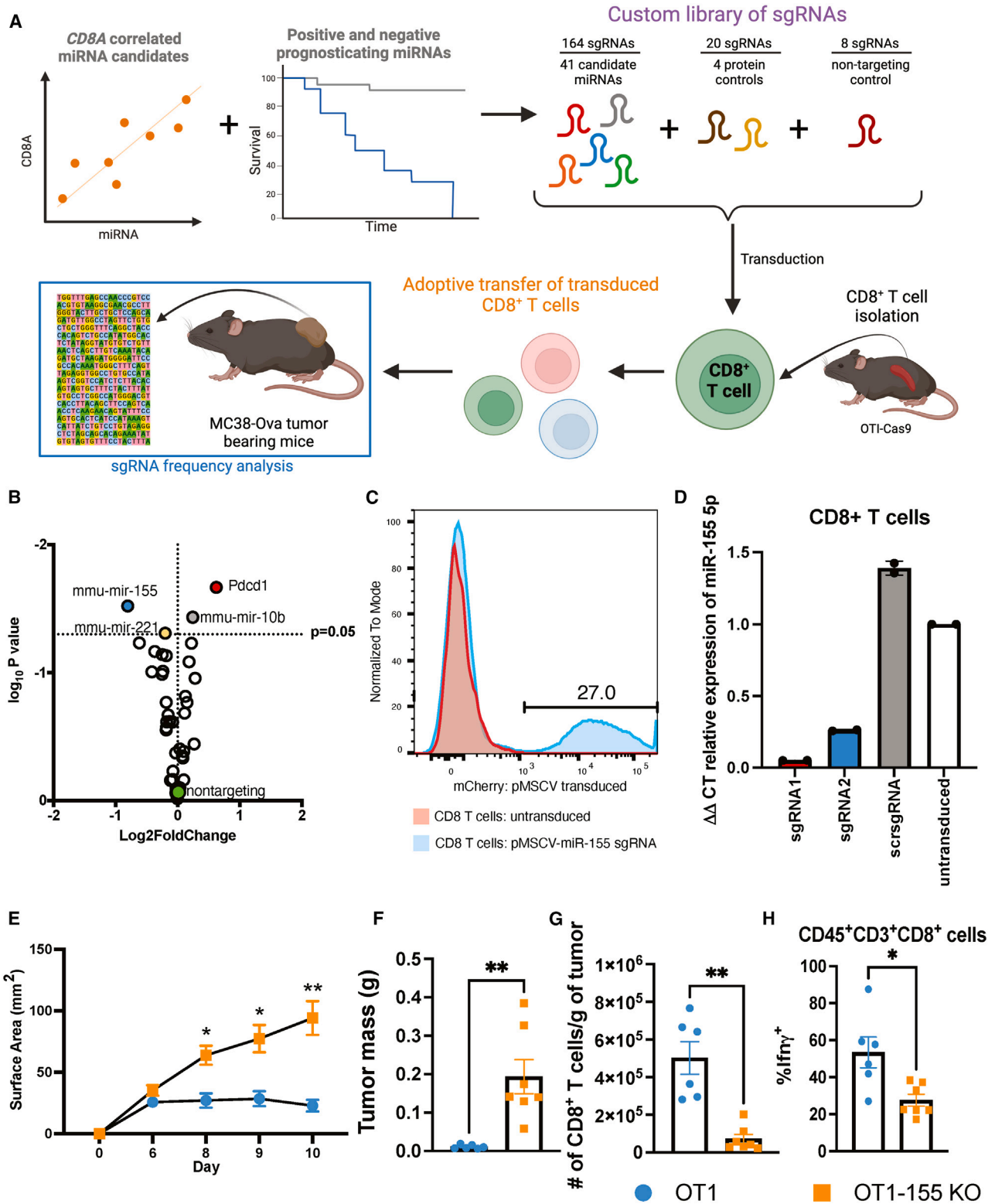


Figure 1. A functional *in vivo* screen targeting miRNAs identifies miR-155 as selectively necessary for eff CD8⁺ T cell-mediated anti-tumor immunity

(A) Schematic of the *in vivo* miRNA CRISPR-Cas9 screen. miRNAs were selected based on positive correlation with *CD8A* in COAD and TCGA projects with miRNA sequencing data, excluding leukemias and lymphomas, and with positive and negative prognostic power (Cox and Kaplan-Meier [KM] analysis in the legend continued on next page)

effector CD8⁺ T cell persistence.^{25,26} In this study, we found that a single microRNA (miRNA) played a vital role in this entire CD8 T cell differentiation cascade, with each stage playing an indispensable role in anti-tumor immunity and ICI responses.

miRNAs are short non-coding RNAs that inhibit the stability or translation of target messenger RNAs based on sequence complementarity with 3' UTR target sites.³¹ miRNAs are well known to regulate tumor cell biology.³² We and others have found that miRNAs influence distinct immune cells responding to solid tumors^{33–38} and can also impact immunotherapy responses, from ICI³⁵ to chimeric antigen receptor (CAR) T cells.^{39,40} Despite these advances, their potential to predict and influence CRC tumor immunity and immunotherapy responses remains unclear and requires additional investigation.

miRNA-155 (miR-155) has recently emerged as a regulator of tumor immunity due to its influence on a variety of immune cells, including T,^{34,35,41–43} natural killer (NK),⁴⁴ and myeloid cells.⁴⁵ Previously, we found that, in melanoma, an immunologically inflammatory cancer that is highly responsive to ICI therapy, the loss of miR-155 in T cells decreased the accumulation of interferon-gamma⁺ (IFN γ ⁺) CD4⁺ and CD8⁺ T cells and increased tumor growth and burden.^{34,35,41,46} However, the role of miR-155 in immunologically suppressive cancers such as CRC remains understudied.

Through this study on CRC, a classically ICI-resistant cancer, our findings reveal a miR-155-dependent mechanism underlying positive ICI responses. Using an *in vivo* CRISPR-Cas9-based miRNA screen, we identify miR-155 in CD8⁺ T cells as a key regulator of CRC immunity. Loss of miR-155 in murine T cells results in increased CRC tumor burden and a complete loss of ICI response in a normally responsive pre-clinical model. Furthermore, we discovered a dependence on miR-155 for an intratumor CD8⁺ T cell differentiation cascade from Tcf-1⁺ stem-like to Cxcr6⁺ effector states through miR-155 repression of Ship-1 and, subsequently, Tcf-1. Analysis of human CRC patients revealed that miR-155 is primarily expressed in CD8⁺ T cells, correlates with multiple emerging molecular parameters of ICI responses, and is potentially more prognostic than dMMR/MSI-H status, the current clinical standard. Finally, we identified a miR-155-dependent, 15-gene CD8⁺ T cell signature, the “miR-155 15, as a top ICI response predictive signature among 48 publicly available predictive gene signatures across 12 cancer types and 25 independent patient datasets. Together, this work clearly identifies miR-155 as a master regulator of intratumor CD8⁺ T cell responses to CRC tumors, including their capacity to respond to ICI, and these findings have groundbreaking translational implications for how we diagnose and treat CRC.

RESULTS

miR-155 is the most functionally significant miRNA in CD8⁺ T cells in murine colon cancer

To identify miRNA determinants of CD8⁺ T cell-mediated CRC immunity and ICI responses, we performed an *in vivo* tumor antigen-specific CD8⁺ T cell CRISPR-Cas9 miRNA screen. We selected miRNAs that positively correlated with CD8A in colon adenocarcinoma (COAD), skin cutaneous melanoma (SKCM), and non-immunologic or hematopoietic origin cancer types with miRNA sequencing data from The Cancer Genome Atlas (TCGA) projects. Additionally, we included miRNAs correlated with patient survival in immune-enriched SKCM, where the immune infiltration was validated with TCGA data at the transcriptomic, protein, and pathologic levels.⁴⁷ We referenced this SKCM subtype because it is among the most thoroughly validated immune-enriched cancer subtypes based on TCGA data. Using this process, we identified 41 candidate miRNAs and created a custom library of single guide RNAs (sgRNAs) targeting these miRNAs, 5 protein controls, and scrambled controls. The library was transduced into OT1-Cas9-CD8⁺ T cells, which have a transgenic T cell receptor (TCR) recognizing ovalbumin (OVA). The transduced CD8⁺ T cells were adoptively transferred into TCR β knockout (TCR β KO) mice, which lack CD4⁺ and CD8⁺ T cells, 7 days post challenge with MC38-OVA cells (a syngeneic COAD cell line expressing OVA). CD8⁺ T cell function/persistence/infiltration were then determined from the frequency of sgRNA barcodes targeting each miRNA in tumors compared to input barcode frequencies in the adoptively transferred CD8⁺ T cells (Figure 1A). The sgRNAs targeting genes inhibiting CD8⁺ T cell fitness become enriched, while sgRNAs targeting CD8⁺ T cell fitness genes themselves become depleted (Figures 1A and 1B). *Pdcd1* (PD-1) sgRNA barcodes showed the highest statistically significant enrichment, validating this functional screen, as PD-1 is a known inhibitor of T cell function and clinical target of ICI. In contrast, miR-155 sgRNA barcodes showed the highest statistically significant depletion (Figure 1B). The similarity in the magnitude of change of miR-155 and *Pdcd1* sgRNA barcode representation highlights the importance of miR-155 as the most impactful miRNA positive regulator of CD8⁺ T cell TME accumulation. Within our system, we had a ~30% transduction efficiency (Figure 1C) and successfully deleted target genes in mCherry⁺ transduced sorted cells (Figure 1D). In TCR β KO mice challenged with MC38-OVA cells, miR-155⁺CD8⁺ OT1 cells (wild type [WT]) elicited nearly complete tumor clearance, while OT1-miR-155KO-CD8⁺ T cell recipients could not control tumor growth or burden (Figures 1E and

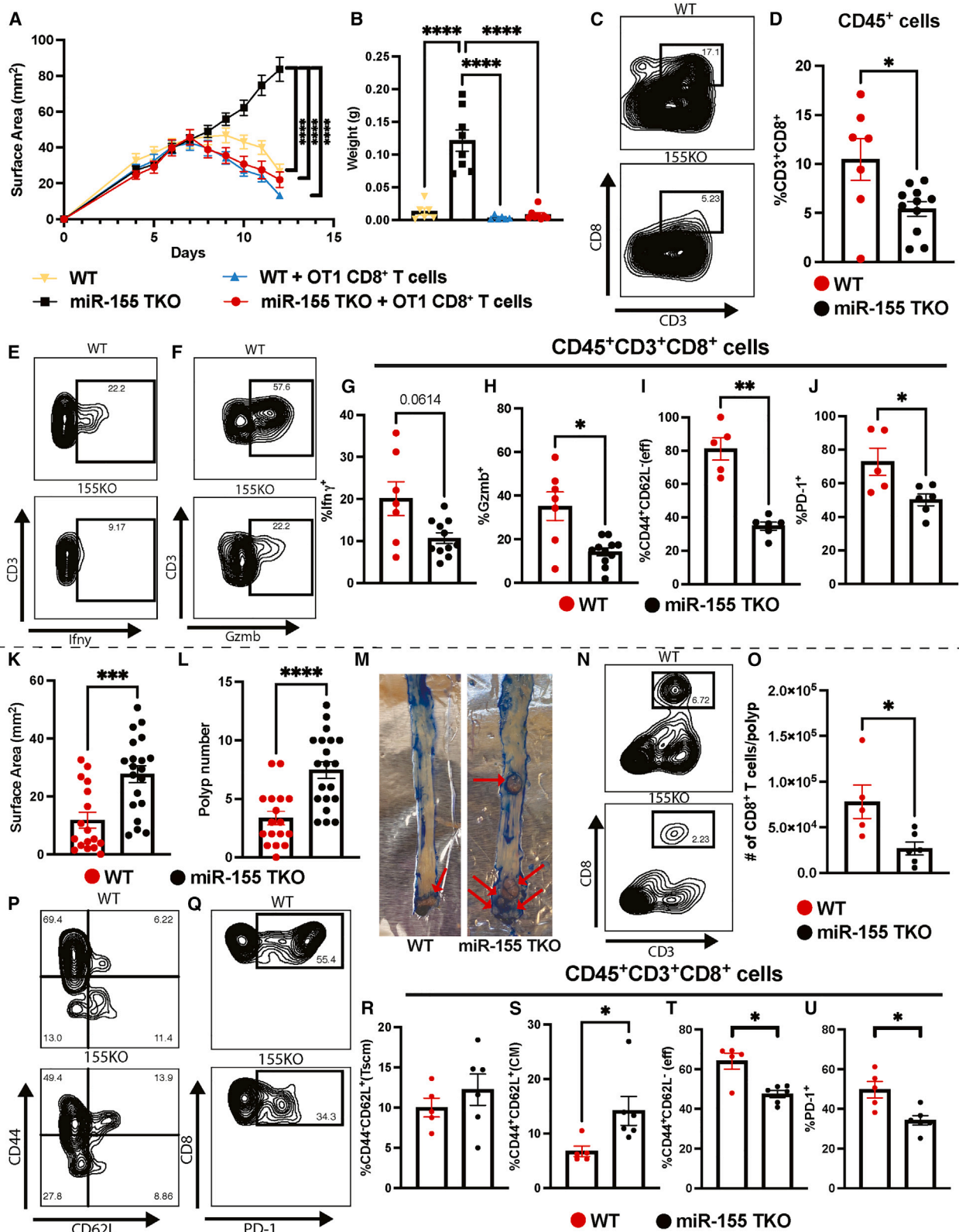
SKCM-immune or cell-type identification by estimating relative subsets of RNA transcripts [CIBERSORT]-CD8a-high cohort). 2E5 mCherry⁺ (library-transduced) cells were adoptively transferred intravenously (i.v.) into TCR β KO mice 7 days post challenge with 1E6 MC38-OVA cells subcutaneously.

(B) PCR barcode enrichment quantification with log2fold change normalized to input sgRNA barcode representation; one sample t and Wilcoxon tests; dashed line, $p = 0.05$; $n = 4$.

(C and D) Representative mCherry⁺ FACs of transduced CD8⁺ T cells with psMSCV-miR-155 sgRNA (C) relative expression of miR-155-5p in mCherry⁺ CD8⁺ T cells ($n = 2$) (D).

(E–H) TCR β KO mice challenged with MC38-OVA cells and given 2E5 OT1 or OT1-miR155 KO (OT1-155KO) CD8⁺ T cells i.v.; $n = 6–8$ per group; tumor growth kinetics (E), tumor mass (F), number of CD8⁺ T cells/g of tumor (G), percentage of IFN γ ⁺ CD8⁺ T cells (H); two-way ANOVA with multiple comparisons; t test with Welch's correction; * $p > 0.05$, ** $p > 0.01$. Bars represent mean; error bars represent SEM.

See also Figure S1.



(legend on next page)

1F), validating miR-155 as an intrinsic regulator of tumor-antigen specific CD8⁺ T cells. Additionally, miR-155KO in OT1 CD8⁺ T cells reduced the frequency and number of intratumoral- and IFN γ ⁺-CD8⁺ T cells and decreased *in vitro* cytotoxic function against MC38-OVA cells (Figures 1G–1H, S1A, S1B, S1D, and S1E). The expansion and functional deficits were restricted to the TME and not the tdLNs and reflected an intratumoral reduction in effector (eff) CD44⁺CD62L⁻ CD8⁺ T cells and corresponding expansion of central memory-like (CM) CD44⁺CD62L⁺ CD8⁺ T cells (Figures S1C and S1E–S1H), which have stem-like properties, are highly proliferative, and are precursors of expanding eff CD8⁺ T cells.^{28,48–52} Despite this increased CD8⁺ CM pool, miR-155 KO CD8⁺ T cells failed to expand and terminally differentiate into anti-tumor eff CD8⁺ T cells. Together, these findings identify miR-155 as the most significant miRNA positively regulating CD8⁺ T cell anti-tumor immunity against CRC, which selectively occurs intratumorally.

T cell-intrinsic miR-155 is necessary for anti-tumor immunity in pre-clinical colon cancer models

We next examined whether T cell miR-155 status was relevant in mutationally distinct pre-clinical CRC murine models representative of two of four CRC molecular subtypes.¹³ We examined both MSI-H and colitis-associated CRC, which is characterized by an immune-suppressive TME.^{13,53–55} To test the necessity of miR-155, we utilized CD4-Cre⁺ miR-155fl/fl mice (miR-155 T cell conditional KO [TKO]), knocking out miR-155 in CD4⁺ and CD8⁺ T cells, and miR-155 fl/fl (WT) littermate controls for the syngeneic MC38 model (MSI-H)⁵⁶ or the azoxymethane (AOM)/dextran sodium sulfate (DSS) model (colitis-associated CRC). miR-155 TKO mice challenged with MC38-OVA could not control tumor growth (Figure 2A) or overall burden (Figure 2B). Tumor control in miR-155 TKO mice was restored to WT levels with an adoptive transfer of miR-155⁺ OT1-CD8⁺ T cells (Figures 2A and 2B). We also found a lower frequency of intratumoral CD8⁺ T cells and IFN γ ⁺ and Gzmb⁺ CD8⁺ T cells in miR-155 TKO mice (Figures 2C–2H). Additionally, miR-155 TKO mice had a decreased frequency of PD-1⁺ and eff CD8⁺ T cells, indicating antigen-experienced tumor-associated T cells and eff anti-tumor responses^{57–59} (Figures 2I and 2J). This decreased eff population is likely due to a failure in differentiation from the T stem cell-like memory (Tscm) or CM states, both of which are expanded in miR-155 TKO mice (Figures S2A and S2B). T cell miR-155 minimally impacted the frequency of tumor-associated NK and NK T cells (Figures S2D and S2E). Loss of T cell miR-155 also modestly decreased the frequency of IFN γ ⁺ CD4⁺ T cells without any impact on the frequency of CD4⁺ T cells (Figures S2C and

S3B). A trending decrease in M1 macrophages was also noted when T cells lacked miR-155 (Figure S3C).

Similar to the MC38 model, when challenged with AOM/DSS, miR-155 TKO mice have an increased tumor burden and polyp numbers (Figures 2K–2M). These mice also have a decreased frequency of total CD8⁺ T cells, PD-1⁺ CD8⁺ T cells, and eff CD8⁺ T cells and an increased frequency of CM CD8⁺ T cells (Figures 2N–2U and S2M). Notably, these stark immunologic differences were restricted to tumors and not seen in the spleen in the MC38 model or AOM/DSS tdLNs (Figures S2F–S2L and S2V–S2Y). Similar to the MC38 model, miR-155 TKO mice challenged with AOM/DSS exhibited an unchanged frequency of NK and NKT cells, including Gzmb⁺ cells, but showed a trending decrease in IFN γ ⁺ cells (Figures S2P–S2U). miR-155 TKO also decreased the frequency of IFN γ ⁺ CD4⁺ T cells without any impact on the frequency of CD4⁺ T cells (Figures S2N and S2O). Regardless of the colon cancer subtype, our data indicate that T cell miR-155 is crucial in promoting the expansion, anti-tumor function, and accumulation of intratumoral eff CD8⁺ T cells and that miR-155⁺ CD8⁺ T cells are sufficient for mediating this antitumor response, which appears to involve additional immune cells. However, it remains unclear whether T cell miR-155 impacts ICI responses.

T cell-intrinsic miR-155 is necessary for ICI responses in a pre-clinical colon cancer model

To determine whether miR-155 regulates CRC ICI responses, we challenged WT and miR-155 TKO mice with MC38 cells and administered either PBS or anti-PD-1 monoclonal antibody (mAb) therapy (ICI). miR-155 TKO mice treated with PBS or ICI exhibited equivalent tumor growth kinetics and mass (Figures 3A and 3B), consistent with an unchanged frequency and number of CD8⁺ T cells/g of tumor (Figures 3C, 3D, and S3A). Meanwhile, WT mice given ICI exhibited significantly less growth and nearly complete tumor regression compared to WT mice treated with PBS (Figures 3A and 3B). ICI therapy could not rescue the defective eff CD8⁺ T cell numbers, differentiation, or eff responses of miR-155 TKO mice to those seen in WT mice (Figures 3D–3P and S3A). However, ICI therapy marginally improved features of eff CD8⁺ T cell differentiation in miR-155 TKO mice, as seen with the contraction of TME CD8⁺ Tscm cells (Figures 3M and 3N) and the expansion of TME Gzmb⁺ (Figures 3E–3G), PD-1⁺ (Figures 3I–3K), and eff CD8⁺ T cells (Figures 3M and 3P) as well as tdLN Gzmb⁺CD8⁺ T cells (Figure S3I). Despite some modest functional responses, miR-155KO CD8⁺ T cells could not effectively persist in the tumor and/or transition into antigen-experienced PD-1⁺ (Figure 3K),

Figure 2. T cell miR-155 promotes eff T cell-mediated antitumor immunity in two molecular subtypes of colon cancer

(A and B) Tumor growth kinetics (A) and tumor mass (B) of miR-155fl/fl (WT) or miR-155fl/fl CD4Cre⁺ (miR-155 TKO) mice challenged with MC38-OVA cells and given 2E5 OT1 CD8⁺ T cells or PBS i.v. 3 days post-injection (d.p.i.); *n* = 6–8.

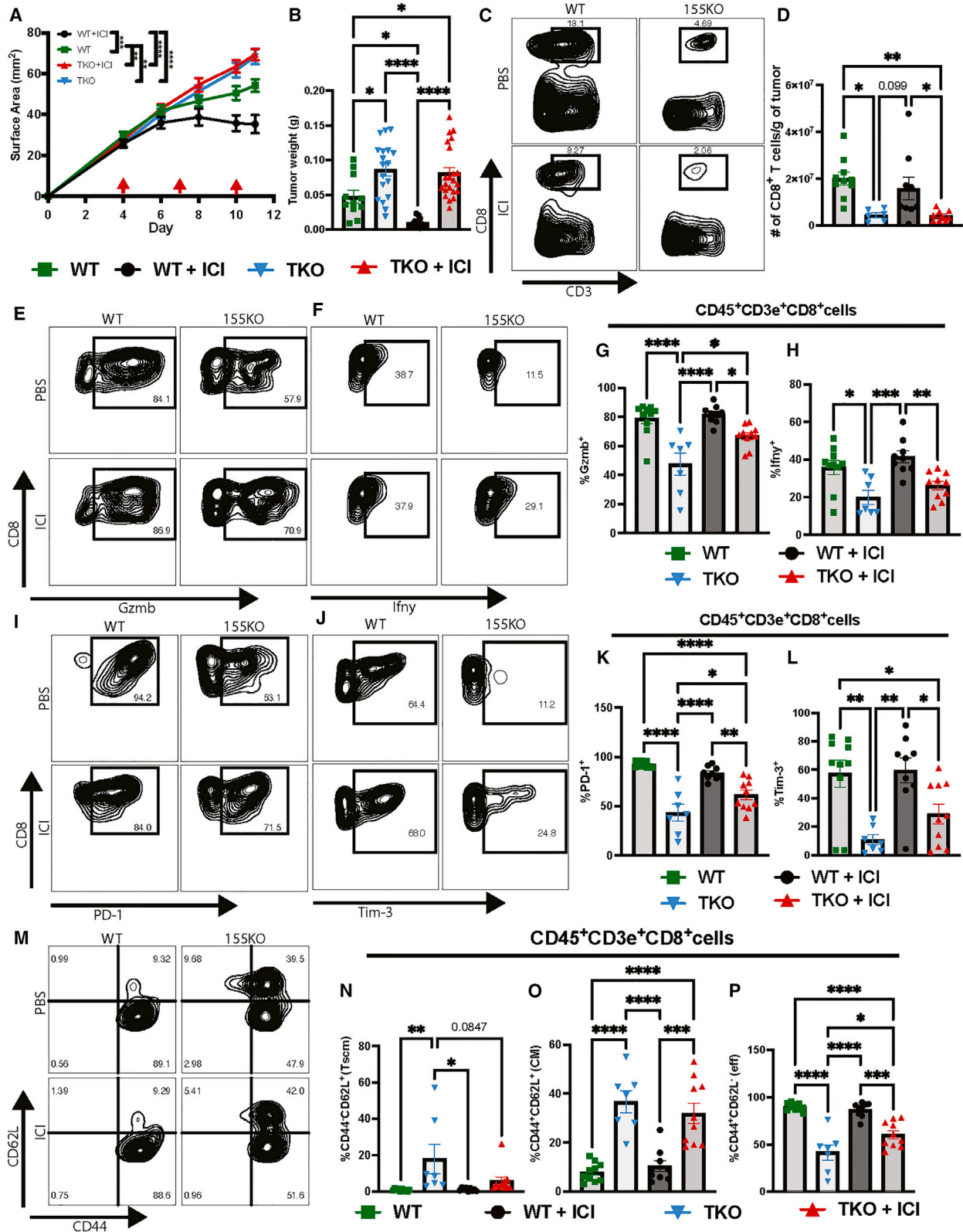
(C–H) Frequency of intratumoral CD8⁺ T cells (C and D), IFN γ ⁺ (E and G), and Gzmb⁺ (F and H) in WT or miR-155 TKO mice challenged with MC38 cells; *n* = 7–11.

(I and J) Frequency of intratumoral eff CD44⁺CD62L⁻ (I) and PD-1⁺ (J) CD8⁺ T cells in WT or miR-155 TKO mice challenged with MC38-OVA cells; *n* = 5–6.

(K–M) Tumor area measurements (K) and polyp count (L) of WT or miR-155 TKO mice challenged with AOM/DSS (M). Data were pooled from two replicate experiments; *n* = 17–20.

(P–U) Frequency and number of CD8⁺ T cells/g of tumor (N and O) and frequency of intratumoral Tscm CD44⁻CD62L⁺ (P and R), CM CD44⁺CD62L⁺ (P and S), eff CD44⁺CD62L⁻ (P and T), and PD-1⁺ (Q and U) CD8⁺ T cells; *n* = 5–6.

t test with Welsh's correction; **p* > 0.05, ***p* > 0.01. Bars represent mean; error bars represent SEM. See also Figure S2.



(legend on next page)

Tim-3⁺ (Figure 3L),⁶⁰ or eff CD8⁺ T cell states (Figure 3P) necessary for high CD8⁺ T cell TME infiltration and ICI response.^{50,61} This was corroborated by an expanded pool of Tscm and CM CD8⁺ T cells in miR-155 KO mice (Figures 3M–3P). In the tdLNs of WT and miR-155 TKO mice, there were little to no differences (<2%) in the frequency of CD8⁺ T cells as well as naive, CM, eff, PD-1⁺, Tim-3⁺, IFN γ ⁺, and Gzmb⁺ CD8⁺ T cells (Figures S3D–S3K). These results show that miR-155 is necessary for intratumoral eff CD8⁺ T cell differentiation and persistence to elicit proper antitumor and ICI responses.

T cell miR-155 enables the intratumoral CD8⁺ T cell stem-like-to-eff differentiation in colon cancer

To better understand the T cell states within colon cancer, we performed single-cell RNA sequencing (scRNA-seq) on CD45⁺ TME immune cells sorted from MC38-challenged WT or miR-155 TKO mice with or without ICI (Figure 4A). The most dramatic change was in the frequency of the CD8⁺ T cell cluster, approximately 5-fold lower in miR-155 TKO immune cells (Figures 4A and S4A). Upon differential gene analysis, we saw an enrichment of eff-related genes in miR-155⁺ CD8⁺ T cells, such as *Id2*, *Pdcd1*, *Lag3*, and *Nkg7*, among many others, compared to miR-155 TKO CD8⁺ T cells. Most notable was an increase in *Cxcr6* expression, as recent literature illustrates its role in eff CD8⁺ T cell TME persistence, cytotoxic T lymphocyte (CTL)-mediated antitumor immunity, and necessity for ICI responses.^{25,26} There was also a trending increase in *Cxcr6* expression and eff genes, such as *Prf1*, *Tnfrsf9* (4-1BB), and *Tbx21* (Tbet) in WT+ICI versus WT (no ICI) CD8⁺ T cells (Figures S4B–S4F), confirming a response to ICI treatment. Of downregulated genes, *Tcf7* (Tcf1), which defines stem-like T cells, was the most significantly downregulated in WT CD8⁺ T cells with or without ICI (Figures 4B and S4C). We validated these findings in miR-155 KO or WT animals challenged with MC38 cells. Again, the frequency and number of tumor-associated miR-155KO CD8⁺ T cells decreased, which resulted in a greater tumor burden (Figures 4C–4E, S4G, and S4H). Considering intratumoral differentiation of CD8⁺ T cells from Tscm and CM to eff,^{62,63} miR-155KO CD8⁺ T cells were seemingly stuck in the Tscm and CM states with stem-like properties and unable to differentiate into an eff state (Figures 4F–4I). Indeed, these miR-155KO CD8⁺ T cells had expanded stem-like Ccr7⁺Cxcr3r1⁻ and Tcf-1⁺Cxcr6⁻ populations (Figures 4M, 4N, and 4Q). WT CD8⁺ T cells were more differentiated and had expanded proliferative transitory Cx3cr1⁺ and eff Tcf-1⁻Cxcr6⁺ populations (Figures 4M, 4O, and 4P). This stem-like-to-transitory-to-eff differentiation was tumor intrinsic, as no differences were seen in tdLNs (Figures 4R–4U), corroborating the negligible (<2%) changes in the frequency of CD8⁺ T cell and naive, CM, and eff populations in lymphoid tissues across multiple

models of murine CRC (Figures 4J–4L, S4I, S2F, S2J–S2L, and S2V–S2Y). Considering TCR clonality in stem-like and terminally differentiated CD8 T cells in human cancer,⁵⁰ these results are consistent with miR-155 promoting CD8⁺ T cell differentiation of antigen-experienced tdLN primed CD8⁺ T cells necessary for CD8⁺ T cell persistence, tumor immunity, and ICI responses.

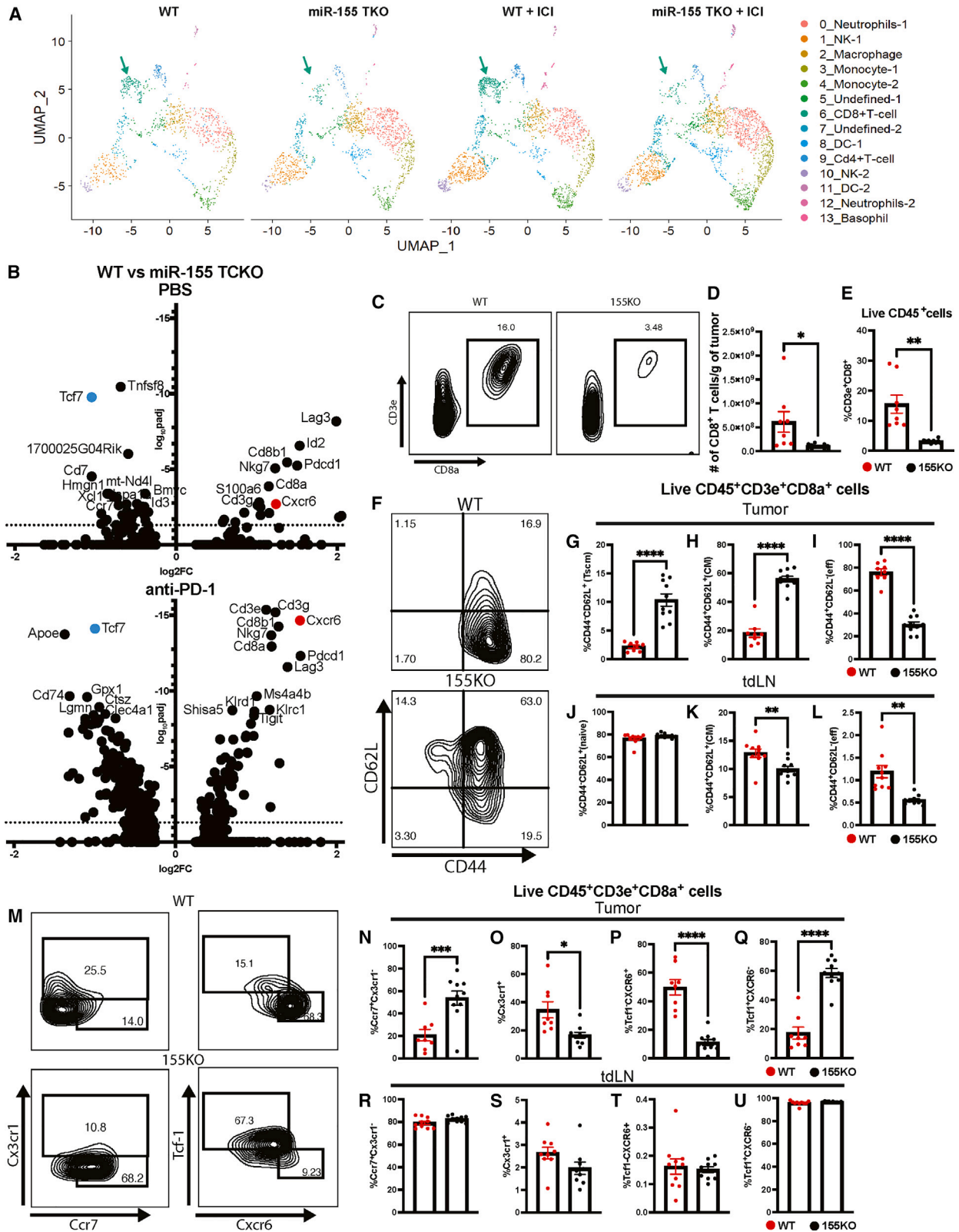
T cell miR-155 represses SHIP-1 (INPP5D), an inhibitor of eff-like CD8⁺ T cell differentiation and antitumor immunity

To understand miR-155-mediated stem-transitory-eff differentiation, we began to examine potential miR-155 targets that could enhance Tcf-1 and have clinical indicators of affecting CRC survival and immunity. We identified the canonical miR-155 target Ship-1 (*Inpp5d*),^{34,64–66} as it met both criteria (Figure 6). Ship-1 inhibits the phosphorylation of Akt (p-Akt) in CD8⁺ T cells and, consequently, eff function.^{65,67–70} Without p-Akt, Foxo-1 remains dephosphorylated, promoting nuclear localization and enhancement of downstream Tcf-1-associated stem-like states in CD8⁺ T cells.^{71–81} In the colon TME, miR-155 KO CD8⁺ T cells, including total, CM, eff, stem-like Ccr7⁺Cx3cr1⁻, and transitory Cx3cr1⁺, had dramatically increased Tcf-1⁺Ship-1⁺ populations (Figures 5A–5D, 5F, and 5G). Additionally, Ship-1 was de-repressed in eff Tcf-1⁻Cxcr6⁺ miR-155 KO CD8⁺ T cells (Figures 5E and 5H). We further examined the relationship between Ship-1 and p-Akt within CD8⁺ T cells throughout the differentiation cascade. Within the activated total, Ccr7⁺ stem-like, Cx3cr1⁺ transitory, and Cxcr6⁺ eff miR-155 KO CD8⁺ T cells, the frequency and expression of p-Akt decreased, while Ship-1 expression increased (Figures 5I and 5J–5M). Phosphorylated Foxo-1 (p-Foxo-1) decreased correspondingly in miR-155 KO CD8⁺ T cells (Figures S5G–S5N), allowing Foxo-1 to skew CD8⁺ T cells toward stem/memory-like states as a transcriptional activator of Tcf-1 (*Tcf7*), *Eomes*, *CD62L* (*Sell*), *Lef1*, and *Klf2*,^{71–81} all of which were upregulated in miR-155 KO CD8⁺ T cells with or without ICI (Figures S4C and S5A–S5D). With these findings, we conclude that miR-155 promotes the eff differentiation cascade for anti-tumor CD8⁺ T cells by inhibiting Ship-1 and subsequently increasing p-Akt. In turn, p-Akt suppresses/phosphorylates Foxo1, which lowers the expression of its target, Tcf-1. Reduced Tcf-1 enables and increases the expression of eff genes such as *Cxcr6*.⁸²

Next, we tested whether Ship1 deletion in *miR-155*^{-/-} CD8⁺ T cells could rescue their defective responses to CRC. Using our CD8⁺ T cell CRISPR-Cas9 platform, Ship1 was deleted in OT1-Cas9-miR-155KO CD8⁺ T cells (Figure S5F). We then adoptively transferred OT1-Cas9, OT1-Cas9-miR-155KO, or OT1-Cas9-miR-155/Ship-1KO CD8⁺ T cells into TCR β KO mice challenged with MC38-OVA cells. Compared to mice receiving

Figure 3. miR-155 is necessary for an effective CD8⁺ T cell-mediated anti-PD-1 response to CRC

(A and B) Tumor growth kinetics (A) and mass (B) of WT or miR-155 TKO mice challenged with MC38 cells and administered ICI or PBS 4, 7, and 10 d.p.i. (red arrows). Data were pooled from two replicate experiments; *n* = 11–22; robust regression and outlier removal (ROUT) outlier test (*Q* = 1%). (C–P) Representative frequency and number of CD8⁺ T cells/g of tumor (C and D) and intratumoral frequency of Gzmb⁺ (E and G), IFN γ ⁺ (F and H), PD-1⁺ (I and K), Tim-3⁺ (J and L), Tscm CD44⁻CD62L⁺ (M and N), CM CD44⁺CD62L⁺ (M and O), and eff CD44⁺CD62L⁻ (M and P) CD8⁺ T cells; *n* = 7–10. One-way ANOVA with multiple comparisons of means of each group; **p* > 0.05, ***p* > 0.01, ****p* > 0.001, *****p* > 0.0001. Bars represent mean; error bars represent SEM. See also Figure S3.



(legend on next page)

OT1-miR-155KO-CD8⁺ T cells, mice receiving OT1-miR-155/Ship-1KO CD8⁺ T cells exhibited greater tumor regression (Figure 5P) and decreased mass (Figure 5Q), partially but significantly restoring the CD8⁺ T cell-mediated tumor control to mice receiving miR-155⁺ OT1-CD8⁺ T cells. This phenotype was complemented by partial rescue of CD8⁺ T cell TME infiltration (Figure 5R), demonstrating a functional consequence for derepressed Ship1 in TME miR-155KO CD8⁺ T cells. Consistent with other tumor-specific phenotypes observed across multiple murine CRC models, WT mice exhibited increased tumoral frequencies of Ki-67⁺ CD8⁺ T cells, indicative of increased proliferation, when compared with their miR-155 TKO counterparts (Figures 5N, 5O, and S5F). Taken together, these data establish an *in vivo* miR-155-dependent repression of Ship1 in the CRC TME that governs a proper CD8⁺ T cell differentiation cascade.

Clinical data implicate SHIP-1 (*INPP5D*) as a miR-155 target and indicator of poor patient and immunologic outcomes

To identify clinically relevant miR-155 targets, we performed Kaplan-Meier survival analysis of all T cell miR-155 validated targets, stratifying patients from TCGA into the top and bottom 30% expressing populations.⁸³ SHIP-1 (*INPP5D*) was among the rare miR-155 targets that conferred a survival advantage when lowly expressed (Figure 6A) and is expressed at different levels across CRC subtypes, with the lowest expression in MSI-H patients (Figure 6B). Additionally, COAD lymphocytes express SHIP-1 protein, making SHIP-1 a clinically relevant CRC-related miR-155 target in lymphocytes (data not shown).⁸⁴ We then performed gene set enrichment analysis (GSEA) on all hallmark pathways and found that *INPP5D* (SHIP-1)-high patients were enriched for the Wnt/ β -catenin pathway, which is a molecular subtype of CRC known to be ICI resistant.⁸⁵ Notably, *INPP5D* (SHIP-1)-low patients were enriched for IFN γ response genes among multiple inflammatory hallmark pathways enriched in miR-155-high patients (Figures 6C and 7E). To confirm this further, we examined an independent cohort of patients with CRC. We found increased expression of SHIP-1 (Figure 6D) and decreased expression of miR-155 in mCRC (N/M positive) (Figure 6E). In non-mCRC (lymph node/metastasis [N/M] negative), miR-155 was more highly expressed and anti-correlated with SHIP-1, but this was lost with metastasis, potentially due to the loss of miR-155-mediated tumor control (Figure 6F). Given the converse relationships between miR-155 and SHIP-1 with GSEA enriched/depleted pathways, MSI-H patient populations

(Figures 6B and 7C), and expression in non-mCRC, CD8⁺ T cell expression of miR-155 is likely repressing SHIP-1 in human CRC, as miR-155 is primarily restricted to CD8⁺ T cells in CRC (Figure 7F).

miR-155 expression defines an anti-tumor CD8⁺ T cell state in colon cancer predictive of pan-cancer ICI responses

Given the recent success of CD8⁺ T cell infiltration (Immunoscore¹⁶) and IFN γ gene signatures¹⁸ in predicting ICI responses, we sought to identify differentially expressed miRNAs in colon cancer using these molecular criteria. We identified miR-155 as the most significantly enriched miRNA in patients expressing high *CD8A*, the primary feature of Immunoscore (Figure 7A). Next, we compared correlations between *CD8A* and miR-155 versus *MLH1* (Figure 7B), an MMR enzyme that is the most prevalent cause of dMMR when hypermethylated.^{87,88} As expected, *MLH1* negatively correlated with *CD8A*. However, a bimodal distribution of patients, one group with *MLH1*-high (proficient MMR/microsatellite stable [MSS]) and another with *MLH1*-low (dMMR/MSI-H), did not allow *MLH1* expression to resolve *CD8A* status within MSI classifiers (Figure 7B). Unlike *MLH1*, a stronger significant positive correlation existed between miR-155 and *CD8A* in all patients and MSI classifiers (Figure 7B). We also examined all other clinically tested MMR enzymes and found no correlation with *CD8A* (Figure S7A). Although dMMR/MSI-H patients had the highest expression of miR-155 (Figure 7C), our results implicate miR-155 as a better indicator of Immunoscore compared to dMMR/MSI-H status, since miR-155 may provide improved resolution in predicting CD8⁺ T cell status irrespective of dMMR/MSI-H status.

Most patients with colon cancer have a wound-healing immune landscape (C1), excluding CD8⁺ T cells from the TME, whereas a smaller proportion of patients have an IFN γ -dominant TME (C2), associated with high CTL levels.¹⁷ Given our preclinical findings, C2 patients unsurprisingly had the highest miR-155 expression (Figure 7D), and upon GSEA, miR-155-high patients had the highest enrichment score for IFN γ response pathway genes among multiple pathways associated with an inflammatory and ICI-responsive TME (Figure 7E). Conversely, the Wnt/ β -catenin pathway, associated with ICI resistance, was enriched in miR-155-low patients (Figure 7E). Of note, this anticorrelates with observations for SHIP1 that are consistent with a functionally relevant miRNA-target relationship (Figure 6C). Using the Human Colon Cancer Atlas scRNA-seq dataset, we also saw that MIR155HG expression

Figure 4. scRNA-seq of tumor-associated immune cells reveals CD8⁺ T cell miR-155 regulation of the Tcf-1/Cxcr6 axis

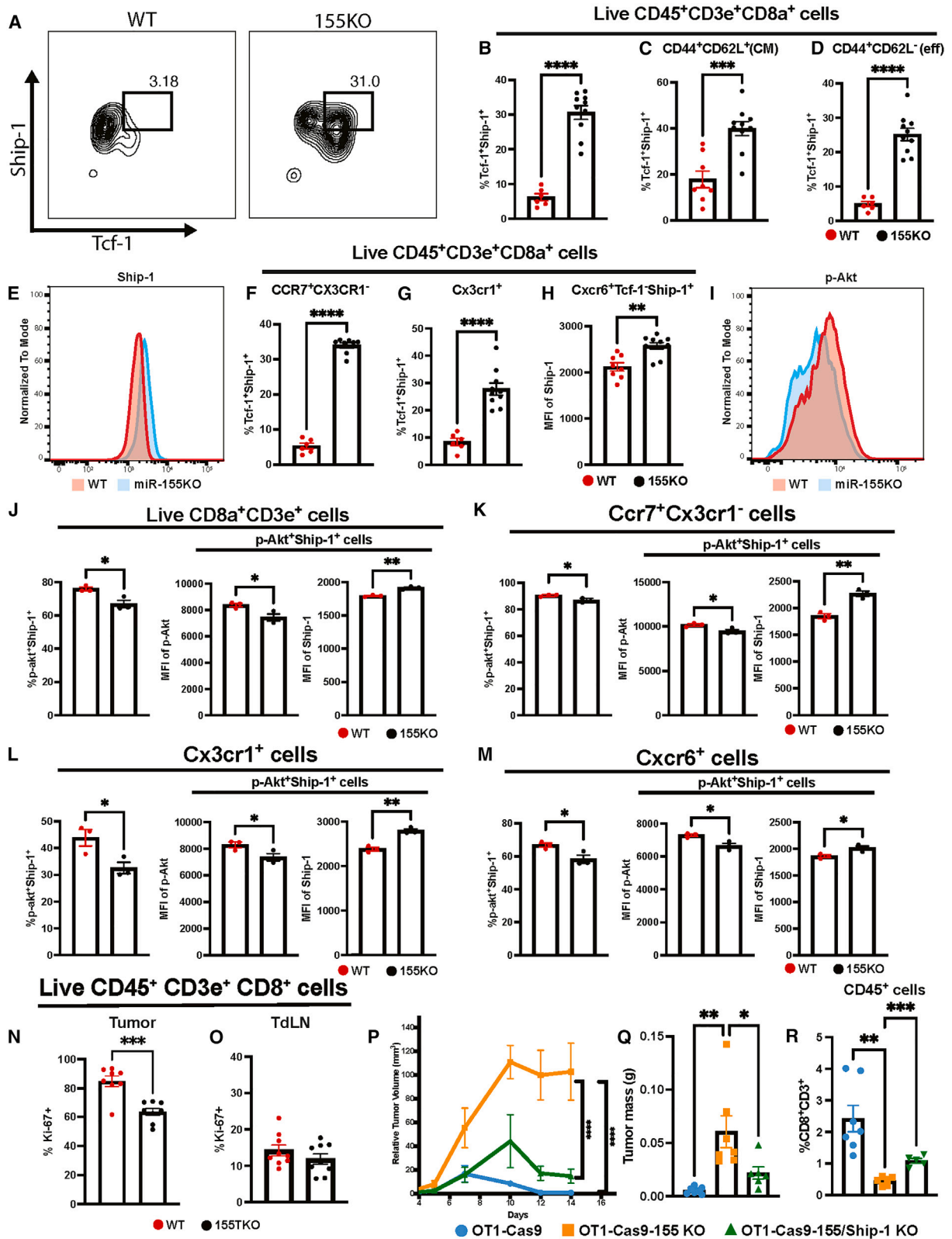
(A) Uniform manifold approximation and projection analysis of tumor-associated CD45⁺ cells from WT or miR-155 TKO mice challenged with MC38 cells and administered anti-Pd-1 mAb (+ICI) or PBS on days 7 and 10 post challenge; teal arrow denotes CD8⁺ T cell cluster.

(B) Log2fold change (log2FC) of gene expression in WT vs. miR-155 TKO CD8⁺ T cell clusters with or without ICI; Wilcoxon rank-sum test with Bonferroni correction.

(C–I and M–Q) *miR-155*^{+/+} (WT) or *miR-155*^{-/-} (155-KO) mice challenged with MC38 cells, frequency and number of tumor-associated CD8⁺ T cells (C–E), and frequencies of intratumoral Tscm CD44⁺CD62L⁺ (F and G), CM CD44⁺CD62L⁺ (F and H), eff CD44⁺CD62L⁻ (F and I), *Ccr7*⁺*Cx3Cr1*⁻ (M and N), *Cx3cr1*⁺ (M and O), *Tcf1*⁻*Cxcr6*⁺ (M and P), and *Tcf1*⁺*Cxcr6*⁻ (M and Q) CD8⁺ T cells.

(J–L, R–U) Frequency of tdLN CD44⁺CD62L⁺ (naive) (J), CM CD44⁺CD62L⁺ (K), eff CD44⁺CD62L⁻ (L), *Ccr7*⁺*Cx3Cr1*⁻ (R), *Cx3cr1*⁺ (S), *Tcf1*⁻*Cxcr6*⁺ (T), and *Tcf1*⁺*Cxcr6*⁻ (U) CD8⁺ T cells.

t test with Welch's correction; **p* > 0.05, ***p* > 0.01, ****p* > 0.001, *****p* > 0.0001. Bars represent mean; error bars represent SEM; *n* = 10 per group. See also Figure S4.



(legend on next page)

is primarily restricted to CD8⁺ T cells, which are the primary IFN γ and major GZMB and PRF1 producers (Figure 7F).⁸⁶ All of these findings suggest that miR-155 is CD8⁺ T cell specific, corresponds to a high Immunoscore and IFN γ responses, and may play a role in the CD8⁺ T differentiation cascade necessary for ICI responses.

We further dissected the impact of miR-155 on ICI responses with a T cell gene signature identified through our scRNA-seq dataset (Figure 4B). We generated a list of 15 genes, which included the overlapping upregulated genes between WT vs. miR-155KO and WT+ICI vs. miR-155KO+ICI in the CD8⁺ T cell cluster plus MIR155HG (Figure 7G). These genes, which we refer to as the miR-155 15 (miR-155_UP), represent a gene set that is highly expressed in miR-155-replete CD8⁺ T cells prior to and during a positive ICI response in our MC38 model. The miR-155 15 were among the top predictive gene signatures of a positive ICI response among 48 publicly available ICI predictive gene signatures across 12 cancer types and 25 patient datasets (Table S1). With a median area under the receiving operating characteristic (AUROC) curve value of 0.70, the miR-155 15 can correctly classify a positive ICI response in 70% of cases. The predictive accuracy of the miR-155 15 is nearly equivalent to the landmark 18 IFN- γ gene signature,¹⁸ and overall, the miR-155 15 are stronger predictors compared to other publicly available ICI response gene signatures (Figures 7H; Table S1) and clinical ICI criteria.^{8–12} Additionally, our gene set is widely detectable and distinct, with minimal overlapping genes compared to other gene signatures, providing an entirely separate means of stratifying a patient's ICI candidacy, which could be used in tandem with other known gene signatures (Figures S6B and S7). Together, our unbiased correlation of miRNAs to CD8A identifies miR-155 as the top CD8⁺ T cell-specific predictor of Immunoscore, an IFN γ dominant landscape, eff CD8⁺ T cells, and ICI correlates. With our miR-155 15 gene signature ranking among the top predictors of ICI responses across 12 cancers, we determined that miR-155 expression in CD8⁺ T cells defines a key biological requirement for an eff CD8⁺ T cell differentiation-driven IFN γ sculpted immune landscape conducive for human ICI responses.

DISCUSSION

Through a functional *in vivo* miRNA CRISPR-Cas9 screen based on clinical parameters, we identified miR-155 as the most impactful positive regulator of tumor-antigen-specific CD8⁺

T cells in colon cancer (Figure 1). To understand the clinical implications of CD8⁺ T cell-expressed miR-155, we studied the role of T cell miR-155 in two preclinical models, each representing a distinct TME,¹³ and within human patients. In our study, T cell miR-155 was a biological requirement for anti-tumor and ICI responses as well as intratumoral CD8⁺ T cell eff differentiation, function, and Cxcr6 expression in immune-promoting and -suppressive TMEs (Figures 1, 2, 3, and 4). miR-155 also defined a CD8⁺ T cell state needed for anti-tumor and ICI responses by multiple molecular parameters in human CRC cohorts. Thus, we conclude that miR-155 acts as a CD8⁺ T cell master regulator, directing differentiation toward an eff anti-tumor state in multiple colon TMEs.

CD8⁺ T cell eff function is often defined as the ability to secrete IFN γ and Gzmb among many other cytolytic molecules. Within the TME, these eff CD8⁺ T cells are needed for anti-tumor and ICI responses. The persistence of eff CD8⁺ T cells is dependent on intratumoral antigen-experienced stem-like populations that originate from primed naive/stem-like CD8⁺ T cells in secondary lymphoid organs.^{19–22,27,28,50} Our data indicate that miR-155 expression in CD8⁺ T cells is necessary for eff function, expansion, and ICI sensitivity in colon cancer (Figures 1, 2, 3, and 4), primarily by facilitating the intratumoral CD8⁺ T cell differentiation from a reservoir of Tscm or CM to eff CD8⁺ T cells.^{89,90} Through scRNA-seq and flow cytometry analysis of intratumoral CD8⁺ T cells, we defined a requirement for miR-155 expression in CD8⁺ T cells for transition from a Tcf-1⁺ stem-like to a Cx3cr1⁺ transitory and then to the terminal Cxcr6⁺ eff state (Figure 4). Although the primary and sustained anti-tumor responses are dependent on Tcf-1⁺ CD8⁺ T cell priming in secondary lymphoid organs, we found little to no differences in the seeding and persistence of adoptively transferred miR-155KO CD8⁺ T cells in tdLNs of T cell-deficient tumor-challenged mice (Figure S1). Additionally, CD8⁺ T cell states in the spleen and tdLNs were unchanged between miR-155 TKO and WT tumor-challenged mice; the miR-155-dependent differentiation cascade was largely limited to the TME (Figures 2, 3, and 4). Without miR-155 expression in CD8⁺ T cells, tumor-associated CD8⁺ T cells could no longer downregulate Tcf-1 to initiate differentiation into an anti-tumor eff state (Figure 4). Given that Tcf-1 directly represses Cxcr6 expression^{82,91,92} we believe that miR-155 is a negative regulator of Tcf-1 that, in turn, promotes eff differentiation and Cxcr6 expression for proper expansion and persistence of intratumoral CD8⁺ T cells.

Figure 5. miR-155 represses Ship-1, indirectly inhibiting Tcf-1 and enhancing anti-tumor immunity

(A–D, F, and G) From WT or 155-KO mice challenged with MC38 cells, frequency of intratumoral Tcf1⁺Ship-1⁺CD8⁺ T cells (A and B) and CM CD44⁺CD62L[−] (C), eff CD44⁺CD62L[−] (D), Ccr7⁺Cx3cr1[−] (F), and Cx3cr1⁺ (G) subsets.

(E and H) Histogram and MFI of Ship-1 in Cxcr6⁺Tcf1[−]Ship-1⁺ CD8⁺ T cells; *n* = 10 per group; t test with Welch's correction.

(I–M) p-Akt⁺ cells (I), frequency of p-Akt⁺Ship-1⁺, and MFI of p-Akt and Ship-1 *in vitro* anti-CD3/CD28 activated CD8⁺ T cells (J) and in Ccr7⁺Cx3cr1[−] (K), Cx3cr1⁺ (L), and Cxcr6⁺ (M) CD8⁺ T cell subsets; *n* = 3 per group; t test with Welch's correction.

(N and O) Ki-67⁺ CD8⁺ T cell frequency from tumor (N) or tdLN (O); *n* = 8–9 per group from WT or miR-155 TKO challenged with MC38 cells; t test with Welch's correction.

(P and Q) Tumor growth (P) and mass (Q) in TCR β KO mice challenged with MC38-OVA cells and given 2E5 OT-1-Cas9 (blue), OT-1-Cas9-miR-155KO (orange), or OT-1-Cas9-miR-155/Ship-1KO (green) CD8⁺ T cells. One-way ANOVA with multiple comparisons of means of each group; *n* = 6–7; Grubbs' outlier test Alpha = 0.01. Frequency of intratumoral CD8⁺ T cells (R); *n* = 5–7; Brown-Forsythe and Welch ANOVA test with multiple comparisons of means of each group. Grubbs' outlier test Alpha = 0.05; **p* > 0.05, ***p* > 0.01, ****p* > 0.001, *****p* > 0.0001. Bars represent mean; error bars represent SEM.

See also Figure S5.

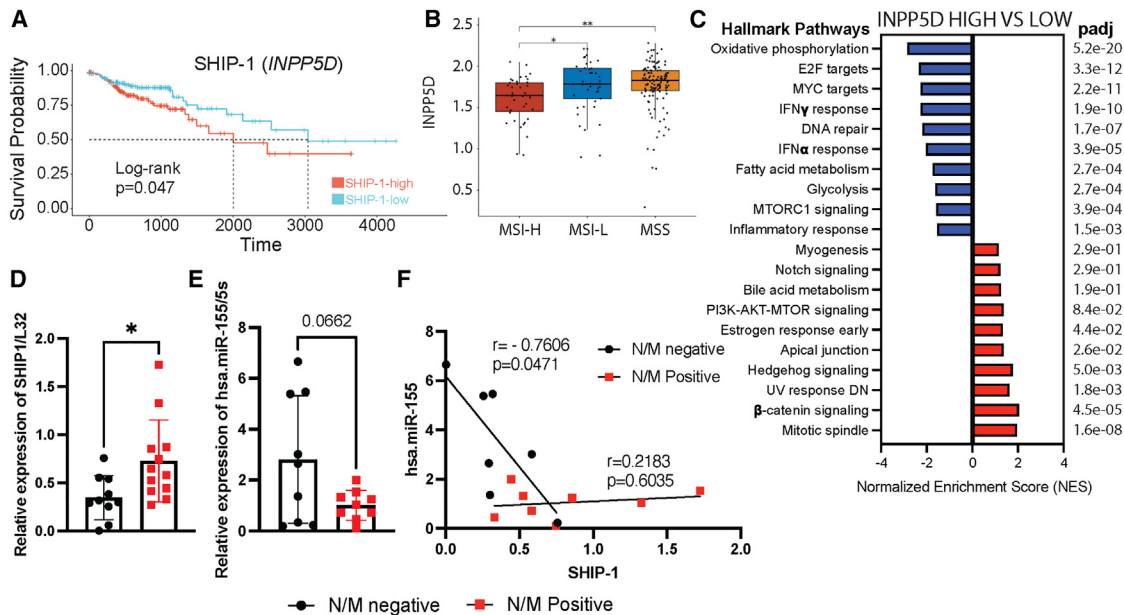


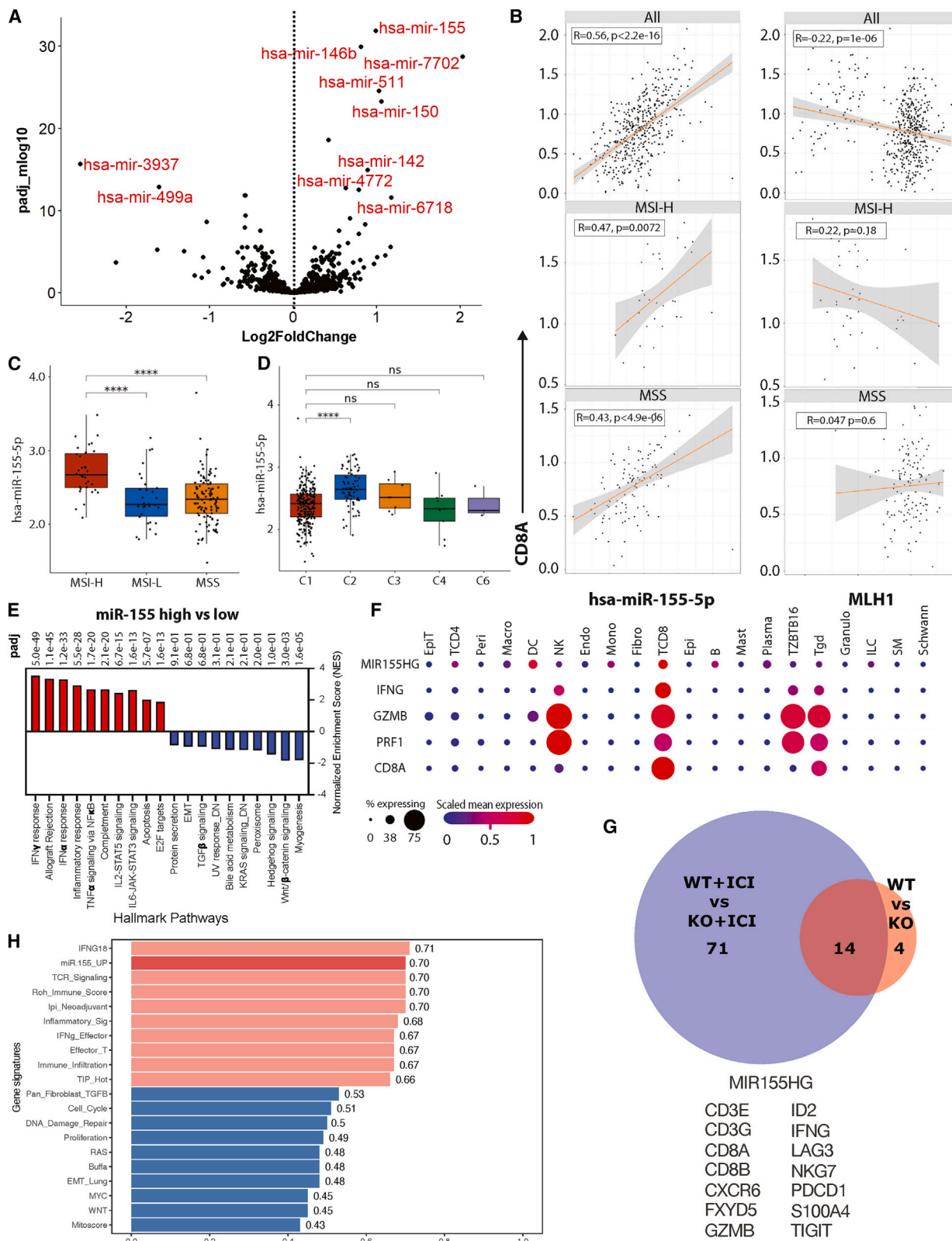
Figure 6. SHIP-1 predicts poor patient outcomes in CRC

(A) Kaplan-Meier's survival probability of COAD patients from TCGA with top and bottom 30% *INPP5D*⁺ patients; *n* = 150 per group. (B) *INPP5D* expression within MSI-H, MSI-L, and MSS TCGA COAD patients. *t* test with pairwise comparisons; **p* > 0.05, ***p* > 0.01. Bars represent mean; error bars represent SE. (C) GSEA of hallmark pathways in top vs. bottom 50% of *INPP5D*⁺ patients; the top 10 and bottom 10 pathways are shown. (D and E) Relative expression of *INPP5D* (SHIP-1)/L32 (D) and hsa-miR-155-5p/L32 (E). *t* test with Welch's correction; **p* > 0.05; Bars represent mean; error bars represent SEM; *n* = 7–11 per group; ROUT outlier test (*Q* = 2%). (F) Computed Pearson correlation coefficients between relative expression of hsa-miR-155-5p/L32 and *INPP5D* (Ship-1)/L32 stratified N/M status.

Each phase of the Tcf-1 stem, Cx3cr1-transitory, and Cxcr6 eff intratumoral CD8⁺ T cell states is crucial for anti-tumor immunity and ICI responses in multiple preclinical models.^{21,24,25,93} Thus, we saw a complete reliance on miR-155 in T cells to elicit an ICI response (Figure 3), as miR-155 facilitated the transition between each CD8⁺ T cell state (Figure 4). Although Tcf-1 is enhanced in miR-155 KO CD8⁺ T cells and widely considered a necessity for anti-tumor and ICI responses,²¹ it has been reported recently that Tcf-1 deficient-CD8⁺ T cells still properly respond to ICI due to an expansion of transitory eff CD8⁺ T cells in highly but not lowly antigenic tumors.²⁷ Considering the dispensable Tcf-1 and mandatory miR-155 requirement for an ICI response in a highly antigenic setting, miR-155 may supersede or complement the biological need for Tcf-1 in ICI in both low- and high-antigen tumor settings, as miR-155 boosts CD8 T cell-mediated tumor immunity against low-affinity tumor antigens.⁴³ miR-155 may also sensitize tumors to anti-PD-1 therapy, as miR-155 expression promoted the expansion of intratumoral PD-1⁺CD8⁺ T cells (Figure 2) and has been reported to promote the persistence of and sustained immunity by PD-1⁺ exhausted CD8⁺ T cells.⁹⁴ Since PD-1 engagement⁹⁵ and loss of miR-155 inhibit the stem-to-eff transition, anti-PD-1 therapy and miR-155 expression are likely synergistic in mediating and maintaining a CD8⁺ T cell-infiltrated TME for durable ICI responses. These findings support and expand on a landmark clinical study showing tumor regression after ICI requiring pre-existing TME-resident CD8⁺ T cells inhibited by the PD-1/PD-L1 axis.⁹⁶

Mechanistically, our data show that miR-155 promotes the critical eff differentiation cascade for anti-tumor CD8⁺ T cells by inhibiting Ship-1, subsequently increasing *p*-Akt, and, in turn, suppressing Foxo1 and lowering expression of Tcf-1 (*Tcf7*). In tumors of miR-155 KO mice, Ship1/Tcf-1 double-positive populations were increased across all CD8⁺ T cell states, and Ship1 was derepressed in rare Cxcr6⁺Tcf-1⁻ differentiated miR-155 KO CD8⁺ T cells. Additionally, all miR-155 KO CD8⁺ T cell states exhibited increased Ship-1 expression and decreased *p*-Akt (Figure 5), which was complemented by Foxo1 activation and Foxo1-enhanced stem/memory factors, including Tcf-1^{67,74,76–81,97,98} (Figures 4Q, S4C, and S4A–4D). We also demonstrate that *in vivo* repression of Ship-1 by miR-155 expands anti-tumor CD8⁺ T cells (Figures 5P–5R). Not only did miR-155 repression of Ship-1 molecularly regulate tumor-associated CD8⁺ T cell stemness and immunity, but clinical CRC data implicate miR-155 repression of SHIP-1 in CD8⁺ T cells in improving anti-tumor immunity and patient outcomes (Figures 6 and 7). Through direct and indirect regulation of CD8⁺ T cell stemness, we conclude that miR-155 promotes CD8⁺ T cell-infiltrated tumors needed for ICI responses.

Corroborating our preclinical models, miR-155 was strongly associated with multiple emerging eff CD8⁺ T cell-driven parameters of ICI responses, specifically Immunoscore and IFN γ responses, and was more correlated with a CD8⁺ T cell-infiltrated tumor compared to all clinically tested dMMR enzymes that



(legend on next page)

identify ICI candidates^{99,100} (Figure 7). We also identified a 15-gene signature, the miR-155 15, that defines an ICI-responsive CD8⁺ T cell state. The miR-155 15 were comparable to the top predictor of ICI responses, as the miR-155 15 can correctly classify an ICI response in 70% of cases (Figures 7G and 7H). As a gene signature, the miR-155-15 delineate basic CD8⁺ T cell biology that is a pre-requisite for a positive ICI therapy response and can thus serve as a biomarker for successful treatment of mCRC among other cancers. The sensitivity and specificity of biomarkers are vital for patient care, as current cancer treatments cause undesirable side effects. With gene signatures like the miR-155 15, we and others can improve patient stratification for ICI, subsequently improving patient outcomes and quality of life.

The miRNA field has made tremendous progress toward our understanding of miRNA production, function, and potential therapeutic application.¹⁰¹ However, miRNAs have been underutilized as a means to boost cancer immunotherapy approaches. By augmenting or inhibiting specific TME cellular miRNAs that impact tumor immunity, miRNAs can improve current and future immunotherapy regimens. Our current study provides key evidence that miR-155 has therapeutic potential in prevalent and deadly cancers such as colon cancer, among others. For instance, CAR T cells face major challenges in solid tumors. Considering the profound impact of miR-155 on solid TME-associated CD8⁺ T cells, CAR T cell function against solid tumors could be optimized by overexpressing miR-155 expression through lentiviral vectors. Alternatively, miR-155 could also be delivered to endogenous TILs via extracellular vesicles or LNPs containing miR-155 to enhance anti-tumor function. Future studies will be critical to identify the synergistic potential of miR-155 with current anti-tumor regimens, including immunotherapy and anti-cancer mRNA vaccines. T cell-produced miRNAs, which our findings have linked to tumor immunity and immunotherapy in the setting of CRC, act to instruct T cells and influence the nature of the TME, both critical and interrelated determinants of effective immunotherapies. Thus, our findings pave the way for the future development of diagnostics and immune therapeutics that target miR-155 in the setting of CRC and other solid tumor types.

Limitations of the study

Our study is focused on the role and mechanism of miR-155 in a critical differentiation cascade in CD8 T cells necessary for anti-tumor immunity and immunotherapy responses. Our model examines the role of miR-155 in tumor-specific CD8 T cells in the presence and absence of CD4 T cells, but we do not fully char-

acterize the contributions of miR-155 in CD4 T cells in this study. Additionally, our mechanistic studies are also limited to pre-clinical models, which do not recapitulate the heterogeneity of human cancers. Last, we correlated our findings to anti-tumor immunity and ICI responsiveness across multiple human cancers; however, we are unable to assess our findings specifically in CD8 T cells across multiple cancer types due to a lack of concurrent scRNA-seq datasets examining immune cells.

RESOURCE AVAILABILITY

Lead contact

Requests for further information, resources, and reagents should be directed to and will be fulfilled by the lead contact, Ryan M. O'Connell (ryan.oconnell@path.utah.edu).

Materials availability

All key resources generated from this study can be made available, if possible, upon request to the lead contact, including plasmids, cell lines, and experimental mouse strains.

Data and code availability

- scRNA-seq data have been deposited at GEO and are publicly available as of the date of publication. The data can be accessed through the identifiers listed in the [key resources table](#). The results published here are in part based upon data generated by the TCGA Research Network (<https://www.cancer.gov/tcga>), Human Protein Atlas,⁸⁴ and Broad Institute Single Cell Portal Human Colon Cancer Atlas (c295).⁸⁶
- Original code comprising the analysis pipeline for the scRNA-seq dataset can be made available upon request to the lead contact.
- Any additional information required to reanalyze the data reported in this paper is available from the lead contact upon request.

ACKNOWLEDGMENTS

We would like to thank the following University of Utah Core Facilities: the HCI-High-Throughput Genomics and Bioinformatics Resources for performing scRNA-seq, the HSC Flow Cytometry Core Facility for cell sorting, and the DNA/Peptide Synthesis Core for primer synthesis. W.W.T. was funded by NIH grant 5F30CA260977, and R.M.O. was funded by NIH grant 5R01AG079477.

AUTHOR CONTRIBUTIONS

The experiments were designed by W.W.T., A.C.T., D.R., M.W., M.J.D., E.J.B., J.L.R., H.A.E., W.P.V., and R.M.O. and completed by W.W.T., B.B., K.M.B., A.M.W., C.B., M.Z.F., A.G., V.T., S.-H.L., B.A., M.C.N., J.T., A.T., C.H., H.A.E., E.S.V., and W.P.V. Human tumor RNA samples were provided by E.J.B. Writing of the manuscript was done by W.W.T. and R.M.O., and it was edited by W.W.T., B.B., K.M.B., A.M.W., W.P.V., H.A.E., and R.M.O. This study was supervised by R.M.O.

Figure 7. miR-155 expression in CD8⁺ T cells is predictive of Immunoscore and IFN γ responses in COAD and ICI responses in human cancer

- (A) Log₂fc miRNA expression in CD8A-high vs. -low COAD patients from TCGA; Wilcoxon rank-sum test with Bonferroni correction.
 (B) Computed Pearson correlation between CD8A and hsa-miR-155-5p and MLH1.
 (C) hsa-miR-155-5p expression within MSI-H, MSI-L, and MSS TCGA COAD patients.
 (D) C1–C6 immune landscapes.¹⁷ t test with pairwise comparisons; *****p* > 0.0001. Bars represent mean; error bars represent SE.
 (E) GSEA of hallmark pathways in top vs. bottom 50% of hsa-miR-155-5p⁺ patients. The top 10 and bottom 10 pathways are shown.
 (F) scRNA-seq scaled mean expression and frequency of MIR155HG, IFNG, GZMB, PRF1, and CD8A within tumor-associated cell types.⁸⁶
 (G) Overlapping significantly upregulated genes between WT vs. miR-155 TKO and WT + ICI vs. miR-155 TKO + ICI in the CD8⁺ T cell cluster from Figure 4G.
 (H) Median AUROC curve value of individual gene signatures across 25 patient datasets and 12 cancers; the top and bottom 10 signatures of 48 are shown. See also Figure S6 and S7 and Table S2.

DECLARATION OF INTERESTS

A provisional patent was filed on October 10, 2024, that is related to the miR-155 gene signature being a predictor of responses to ICI (U-8545).

STAR★METHODS

Detailed methods are provided in the online version of this paper and include the following:

- **KEY RESOURCES TABLE**
- **EXPERIMENTAL MODEL AND STUDY PARTICIPANT DETAILS**
 - Mice
 - Tumor cell lines
- **METHOD DETAILS**
 - Tumor models
 - Administration of anti-PD-1
 - Single-cell RNA sequencing and sample preparation
 - qPCR analysis of miR-155-5p and *INPP5D*
 - Human colon cancer scRNAseq analysis
 - Analysis of SHIP-1 protein expression in human patients with cancer
 - CD8 T cell antitumor miRNA CRISPR target collection
 - Amplicon seq of integrated CRISPR library barcode sequences
 - Retroviral generation and viral transduction
 - CD8 T cell isolation and preparation for *in vivo* and *in vitro* use
 - Flow cytometric analysis of single cells from lymphoid organs and tumors
 - Western blot protocol
 - Block/probe conditions
- **QUANTIFICATION AND STATISTICAL ANALYSIS**
 - Statistics
 - Collection of publicly available transcriptome expression dataset and gene signature profiles related to immunotherapy response
 - Calculation of gene signature performance in predicting immunotherapy response
 - The Cancer Genome Atlas (TCGA) patient data analysis

SUPPLEMENTAL INFORMATION

Supplemental information can be found online at <https://doi.org/10.1016/j.celrep.2025.115301>.

Received: August 4, 2024

Revised: November 24, 2024

Accepted: January 22, 2025

Published: February 12, 2025

REFERENCES

1. Ahnen, D.J., Wade, S.W., Jones, W.F., Sifri, R., Mendoza Silveiras, J., Greenamyre, J., Guiffre, S., Axilbund, J., Spiegel, A., and You, Y.N. (2014). The increasing incidence of young-onset colorectal cancer: a call to action. *Mayo Clin. Proc.* 89, 216–224. <https://doi.org/10.1016/j.mayocp.2013.09.006>.
2. Arnold, M., Sierra, M.S., Laversanne, M., Soerjomataram, I., Jemal, A., and Bray, F. (2017). Global patterns and trends in colorectal cancer incidence and mortality. *Gut* 66, 683–691. <https://doi.org/10.1136/gutjnl-2015-310912>.
3. Siegel, R.L., Wagle, N.S., Cercek, A., Smith, R.A., and Jemal, A. (2023). Colorectal cancer statistics, 2023. *CA A Cancer J. Clin.* 73, 233–254. <https://doi.org/10.3322/caac.21772>.
4. Heinemann, V., von Weikersthal, L.F., Decker, T., Kiani, A., Vehling-Kaiser, U., Al-Batran, S.E., Heintges, T., Lerchenmüller, C., Kahl, C., Seipelt, G., et al. (2014). FOLFIRI plus cetuximab versus FOLFIRI plus bevacizumab as first-line treatment for patients with metastatic colorectal cancer (FIRE-3): a randomised, open-label, phase 3 trial. *Lancet Oncol.* 15, 1065–1075. [https://doi.org/10.1016/S1470-2045\(14\)70330-4](https://doi.org/10.1016/S1470-2045(14)70330-4).
5. Cogdill, A.P., Andrews, M.C., and Wargo, J.A. (2017). Hallmarks of response to immune checkpoint blockade. *Br. J. Cancer* 117, 1–7. <https://doi.org/10.1038/bjc.2017.136>.
6. Le, D.T., Uram, J.N., Wang, H., Bartlett, B.R., Kemberling, H., Eyring, A.D., Skora, A.D., Luber, B.S., Azad, N.S., Laheru, D., et al. (2015). PD-1 Blockade in Tumors with Mismatch-Repair Deficiency. *N. Engl. J. Med.* 372, 2509–2520. <https://doi.org/10.1056/NEJMoa1500596>.
7. Oliveira, A.F., Bretes, L., and Furtado, I. (2019). Review of PD-1/PD-L1 Inhibitors in Metastatic dMMR/MSI-H Colorectal Cancer. *Front. Oncol.* 9, 396. <https://doi.org/10.3389/fonc.2019.00396>.
8. McGrail, D.J., Pilié, P.G., Rashid, N.U., Voorwerk, L., Slagter, M., Kok, M., Jonasch, E., Khasraw, M., Heimberger, A.B., Lim, B., et al. (2021). High tumor mutation burden fails to predict immune checkpoint blockade response across all cancer types. *Ann. Oncol.* 32, 661–672. <https://doi.org/10.1016/j.annonc.2021.02.006>.
9. Overman, M.J., McDermott, R., Leach, J.L., Lonardi, S., Lenz, H.-J., Morse, M.A., Desai, J., Hill, A., Axelson, M., Moss, R.A., et al. (2017). Nivolumab in patients with metastatic DNA mismatch repair-deficient or microsatellite instability-high colorectal cancer (CheckMate 142): an open-label, multicentre, phase 2 study. *Lancet Oncol.* 18, 1182–1191. [https://doi.org/10.1016/s1470-2045\(17\)30422-9](https://doi.org/10.1016/s1470-2045(17)30422-9).
10. Overman, M.J., Lonardi, S., Wong, K.Y.M., Lenz, H.-J., Gelsomino, F., Aglietta, M., Morse, M., Van Cutsem, E., McDermott, R.S., Hill, A.G., et al. (2019). Nivolumab (NIVO) + low-dose ipilimumab (IPI) in previously treated patients (pts) with microsatellite instability-high/mismatch repair-deficient (MSI-H/dMMR) metastatic colorectal cancer (mCRC): Long-term follow-up. *J. Clin. Oncol.* 37, 635. https://doi.org/10.1200/JCO.2019.37.4_suppl.635.
11. Le, D.T., Uram, J.N., Wang, H., Bartlett, B.R., Kemberling, H., Eyring, A.D., Skora, A.D., Luber, B.S., Azad, N.S., Laheru, D., et al. (2015). PD-1 Blockade in Tumors with Mismatch-Repair Deficiency. *N. Engl. J. Med.* 372, 2509–2520. <https://doi.org/10.1056/nejmoa1500596>.
12. Le, D.T., Kim, T.W., Van Cutsem, E., Geva, R., Jäger, D., Hara, H., Burge, M., O’Neil, B., Kavan, P., Yoshino, T., et al. (2020). Phase II Open-Label Study of Pembrolizumab in Treatment-Refractory, Microsatellite Instability–High/Mismatch Repair–Deficient Metastatic Colorectal Cancer: KEYNOTE-164. *J. Clin. Oncol.* 38, 11–19. <https://doi.org/10.1200/jco.19.02107>.
13. Guinney, J., Dienstmann, R., Wang, X., de Reyniès, A., Schlicker, A., Sonnen, C., Marisa, L., Roepman, P., Nyamundanda, G., Angelino, P., et al. (2015). The consensus molecular subtypes of colorectal cancer. *Nat. Med.* 21, 1350–1356. <https://doi.org/10.1038/nm.3967>.
14. Westcott, P.M.K., Muyas, F., Hauck, H., Smith, O.C., Sacks, N.J., Ely, Z.A., Jaeger, A.M., Rideout, W.M., Zhang, D., Bhutkar, A., et al. (2023). Mismatch repair deficiency is not sufficient to elicit tumor immunogenicity. *Nat. Genet.* 55, 1686–1695. <https://doi.org/10.1038/s41588-023-01499-4>.
15. Pagès, F., Mlecnik, B., Marliot, F., Bindea, G., Ou, F.-S., Bifulco, C., Lugli, A., Zlobec, I., Rau, T.T., Berger, M.D., et al. (2018). International validation of the consensus Immunoscore for the classification of colon cancer: a prognostic and accuracy study. *Lancet* 391, 2128–2139. [https://doi.org/10.1016/s0140-6736\(18\)30789-x](https://doi.org/10.1016/s0140-6736(18)30789-x).
16. Ghiringhelli, F., Bibeau, F., Greillier, L., Fumet, J.-D., Ilie, A., Monville, F., Laugé, C., Catteau, A., Boquet, I., Majidi, A., et al. (2023). Immunoscore immune checkpoint using spatial quantitative analysis of CD8 and PD-L1 markers is predictive of the efficacy of anti-PD1/PD-L1 immunotherapy in non-small cell lung cancer. *EBioMedicine* 92, 104633. <https://doi.org/10.1016/j.ebiom.2023.104633>.
17. Thorsson, V., Gibbs, D.L., Brown, S.D., Wolf, D., Bortone, D.S., Ou Yang, T.H., Porta-Pardo, E., Gao, G.F., Plaisier, C.L., Eddy, J.A., et al. (2018). The Immune Landscape of Cancer. *Immunity* 48, 812–830.e14. <https://doi.org/10.1016/j.immuni.2018.03.023>.

18. Ayers, M., Lunceford, J., Nebozhyn, M., Murphy, E., Loboda, A., Kaufman, D.R., Albright, A., Cheng, J.D., Kang, S.P., Shankaran, V., et al. (2017). IFN- γ -related mRNA profile predicts clinical response to PD-1 blockade. *J. Clin. Invest.* *127*, 2930–2940. <https://doi.org/10.1172/jci91190>.
19. Fransén, M.F., Schoonderwoerd, M., Knopf, P., Camps, M.G., Hawinkels, L.J., Kneilling, M., Van Hall, T., and Ossendorp, F. (2018). Tumor-draining lymph nodes are pivotal in PD-1/PD-L1 checkpoint therapy. *JCI Insight* *3*, e124507. <https://doi.org/10.1172/jci.insight.124507>.
20. Dammeyer, F., Van Gulijk, M., Mulder, E.E., Lukkes, M., Klaase, L., Van Den Bosch, T., Van Nimwegen, M., Lau, S.P., Latupeirissa, K., Schettler, S., et al. (2020). The PD-1/PD-L1-Checkpoint Restrains T cell Immunity in Tumor-Draining Lymph Nodes. *Cancer Cell* *38*, 685–700.e8. <https://doi.org/10.1016/j.ccell.2020.09.001>.
21. Siddiqui, I., Schaeuble, K., Chennupati, V., Fuentès Marraco, S.A., Calderon-Copete, S., Pais Ferreira, D., Carmona, S.J., Scarpellino, L., Gfeller, D., Pradervand, S., et al. (2019). Intratumoral Tcf1+PD-1+CD8+ T Cells with Stem-like Properties Promote Tumor Control in Response to Vaccination and Checkpoint Blockade Immunotherapy. *Immunity* *50*, 195–211.e10. <https://doi.org/10.1016/j.immuni.2018.12.021>.
22. Connolly, K.A., Kuchroo, M., Venkat, A., Khatun, A., Wang, J., William, I., Hornick, N.I., Fitzgerald, B.L., Damo, M., Kasmani, M.Y., et al. (2021). A reservoir of stem-like CD8(+) T cells in the tumor-draining lymph node preserves the ongoing antitumor immune response. *Sci. Immunol.* *6*, eabg7836. <https://doi.org/10.1126/sciimmunol.abg7836>.
23. Mabrouk, N., Tran, T., Sam, I., Pourmir, I., Gruel, N., Granier, C., Pineau, J., Gey, A., Kobold, S., Fabre, E., and Tartour, E. (2022). CXCR6 expressing T cells: Functions and role in the control of tumors. *Front. Immunol.* *13*, 1022136. <https://doi.org/10.3389/fimmu.2022.1022136>.
24. Yamauchi, T., Hoki, T., Oba, T., Jain, V., Chen, H., Attwood, K., Battaglia, S., George, S., Chatta, G., Puzanov, I., et al. (2021). T-cell CX3CR1 expression as a dynamic blood-based biomarker of response to immune checkpoint inhibitors. *Nat. Commun.* *12*, 1402. <https://doi.org/10.1038/s41467-021-21619-0>.
25. Wang, B., Wang, Y., Sun, X., Deng, G., Huang, W., Wu, X., Gu, Y., Tian, Z., Fan, Z., Xu, Q., et al. (2021). CXCR6 is required for antitumor efficacy of intratumoral CD8⁺ T cell. *J. Immunother. Cancer* *9*, e003100. <https://doi.org/10.1136/jitc-2021-003100>.
26. Di Pilato, M., Kfuri-Rubens, R., Pruessmann, J.N., Ozga, A.J., Messermer, M., Cadilha, B.L., Sivakumar, R., Cianciaruso, C., Warner, R.D., Marangoni, F., et al. (2021). CXCR6 positions cytotoxic T cells to receive critical survival signals in the tumor microenvironment. *Cell* *184*, 4512–4530.e22. <https://doi.org/10.1016/j.cell.2021.07.015>.
27. Escobar, G., Tooley, K., Oliveras, J.P., Huang, L., Cheng, H., Bookstaver, M.L., Edwards, C., Froimchuk, E., Xue, C., Mangani, D., et al. (2023). Tumor immunogenicity dictates reliance on TCF1 in CD8+ T cells for response to immunotherapy. *Cancer Cell* *41*, 1662–1679.e7. <https://doi.org/10.1016/j.ccell.2023.08.001>.
28. Prokhnjevskaja, N., Cardenas, M.A., Valanparambil, R.M., Sobierajska, E., Barwick, B.G., Jansen, C., Reyes Moon, A., Gregorova, P., delBalzo, L., Greenwald, R., et al. (2023). CD8(+) T cell activation in cancer comprises an initial activation phase in lymph nodes followed by effector differentiation within the tumor. *Immunity* *56*, 107–124.e5. <https://doi.org/10.1016/j.immuni.2022.12.002>.
29. Hudson, W.H., Gensheimer, J., Hashimoto, M., Wieland, A., Valanparambil, R.M., Li, P., Lin, J.X., Konieczny, B.T., Im, S.J., Freeman, G.J., et al. (2019). Proliferating Transitory T Cells with an Effector-like Transcriptional Signature Emerge from PD-1(+) Stem-like CD8(+) T Cells during Chronic Infection. *Immunity* *51*, 1043–1058.e4. <https://doi.org/10.1016/j.immuni.2019.11.002>.
30. Zander, R., Schauder, D., Xin, G., Nguyen, C., Wu, X., Zajac, A., and Cui, W. (2019). CD4+ T Cell Help Is Required for the Formation of a Cytolytic CD8+ T Cell Subset that Protects against Chronic Infection and Cancer. *Immunity* *51*, 1028–1042.e4. <https://doi.org/10.1016/j.immuni.2019.10.009>.
31. O'Connell, R.M., Rao, D.S., Chaudhuri, A.A., and Baltimore, D. (2010). Physiological and pathological roles for microRNAs in the immune system. *Nat. Rev. Immunol.* *10*, 111–122. <https://doi.org/10.1038/nri2708>.
32. Testa, U., Pelosi, E., Castelli, G., and Labbaye, C. (2017). miR-146 and miR-155: Two Key Modulators of Immune Response and Tumor Development. *Noncoding RNA* *3*, 22. <https://doi.org/10.3390/ncrna3030022>.
33. He, W., Wang, C., Mu, R., Liang, P., Huang, Z., Zhang, J., and Dong, L. (2017). MiR-21 is required for anti-tumor immune response in mice: an implication for its bi-directional roles. *Oncogene* *36*, 4212–4223. <https://doi.org/10.1038/ncr.2017.62>.
34. Huffaker, T.B., Hu, R., Runtsch, M.C., Bake, E., Chen, X., Zhao, J., Round, J.L., Baltimore, D., and O'Connell, R.M. (2012). Epistasis between microRNAs 155 and 146a during T cell-mediated antitumor immunity. *Cell Rep.* *2*, 1697–1709. <https://doi.org/10.1016/j.celrep.2012.10.025>.
35. Huffaker, T.B., Lee, S.H., Tang, W.W., Wallace, J.A., Alexander, M., Runtsch, M.C., Larsen, D.K., Thompson, J., Ramstead, A.G., Voth, W.P., et al. (2017). Antitumor immunity is defective in T cell-specific microRNA-155-deficient mice and is rescued by immune checkpoint blockade. *J. Biol. Chem.* *292*, 18530–18541. <https://doi.org/10.1074/jbc.M117.808121>.
36. Zhao, E., Maj, T., Kryczek, I., Li, W., Wu, K., Zhao, L., Wei, S., Crespo, J., Wan, S., Vatan, L., et al. (2016). Cancer mediates effector T cell dysfunction by targeting microRNAs and EZH2 via glycolysis restriction. *Nat. Immunol.* *17*, 95–103. <https://doi.org/10.1038/ni.3313>.
37. Zhu, T., Lin, Z., Han, S., Wei, Y., Lu, G., Zhang, Y., Xiao, W., Wang, Z., Jia, X., and Gong, W. (2021). Low miR-16 expression induces regulatory CD4(+)NKG2D(+) T cells involved in colorectal cancer progression. *Am. J. Cancer Res.* *11*, 1540–1556.
38. Tang, W.W., Bauer, K.M., Barba, C., Ekiz, H.A., and O'Connell, R.M. (2022). miR-acylous new avenues for cancer immunotherapy. *Front. Immunol.* *13*, 929677. <https://doi.org/10.3389/fimmu.2022.929677>.
39. Dressel, R., Greinix, H.T., Holler, E., and Dickinson, A.M. (2018). Editorial: Cellular Therapies: Past, Present and Future. *Front. Immunol.* *9*, 1966. <https://doi.org/10.3389/fimmu.2018.01966>.
40. Huang, Q., Xia, J., Wang, L., Wang, X., Ma, X., Deng, Q., Lu, Y., Kumar, M., Zhou, Z., Li, L., et al. (2018). miR-153 suppresses IDO1 expression and enhances CAR T cell immunotherapy. *J. Hematol. Oncol.* *11*, 58. <https://doi.org/10.1186/s13045-018-0600-x>.
41. Ekiz, H.A., Huffaker, T.B., Grossmann, A.H., Stephens, W.Z., Williams, M.A., Round, J.L., and O'Connell, R.M. (2019). MicroRNA-155 coordinates the immunological landscape within murine melanoma and correlates with immunity in human cancers. *JCI Insight* *4*, e126543. <https://doi.org/10.1172/jci.insight.126543>.
42. Dudda, J.C., Salaun, B., Ji, Y., Palmer, D.C., Monnot, G.C., Merck, E., Boudousquie, C., Utschneider, D.T., Escobar, T.M., Perret, R., et al. (2013). MicroRNA-155 is required for effector CD8+ T cell responses to virus infection and cancer. *Immunity* *38*, 742–753. <https://doi.org/10.1016/j.immuni.2012.12.006>.
43. Monnot, G.C., Martinez-Usatorre, A., Lanitis, E., Lopes, S.F., Cheng, W.C., Ho, P.C., Irving, M., Coukos, G., Donda, A., and Romero, P. (2020). miR-155 Overexpression in OT-1 CD8(+) T Cells Improves Anti-Tumor Activity against Low-Affinity Tumor Antigen. *Mol. Ther. Oncolytics* *16*, 111–123. <https://doi.org/10.1016/j.omto.2019.12.008>.
44. Kandell, W.M., Donatelli, S.S., Trinh, T.L., Calescibetta, A.R., So, T., Tu, N., Gilvary, D.L., Chen, X., Cheng, P., Adams, W.A., et al. (2020). MicroRNA-155 governs SHIP-1 expression and localization in NK cells and regulates subsequent infiltration into murine AT3 mammary carcinoma. *PLoS One* *15*, e0225820. <https://doi.org/10.1371/journal.pone.0225820>.
45. Liu, L., Yi, H., He, H., Pan, H., Cai, L., and Ma, Y. (2017). Tumor associated macrophage-targeted microRNA delivery with dual-responsive polypeptide nanovectors for anti-cancer therapy. *Biomaterials* *134*, 166–179. <https://doi.org/10.1016/j.biomaterials.2017.04.043>.

46. Ekiz, H.A., Conley, C.J., Stephens, W.Z., and O'Connell, R.M. (2020). CIPR: a web-based R/shiny app and R package to annotate cell clusters in single cell RNA sequencing experiments. *BMC Bioinf.* *21*, 191. <https://doi.org/10.1186/s12859-020-3538-2>.
47. Akbani, R., Akdemir, K.C., Aksoy, B.A., Albert, M., Ally, A., Amin, S.B., Arachchi, H., Arora, A., Auman, J.T., Ayala, B., et al. (2015). Genomic Classification of Cutaneous Melanoma. *Cell* *161*, 1681–1696. <https://doi.org/10.1016/j.cell.2015.05.044>.
48. Gattinoni, L., Lugli, E., Ji, Y., Pos, Z., Paulos, C.M., Quigley, M.F., Almeida, J.R., Gostick, E., Yu, Z., Carpenito, C., et al. (2011). A human memory T cell subset with stem cell-like properties. *Nat. Med.* *17*, 1290–1297. <https://doi.org/10.1038/nm.2446>.
49. Gong, Y., Suzuki, T., Kozono, H., Kubo, M., and Nakano, N. (2020). Tumor-infiltrating CD62L+PD-1-CD8 T cells retain proliferative potential via Bcl6 expression and replenish effector T cells within the tumor. *PLoS One* *15*, e0237646. <https://doi.org/10.1371/journal.pone.0237646>.
50. Jansen, C.S., Prokhnjevskaja, N., Master, V.A., Sanda, M.G., Carlisle, J.W., Bilén, M.A., Cardenas, M., Wilkinson, S., Lake, R., Sowalsky, A.G., et al. (2019). An intra-tumoral niche maintains and differentiates stem-like CD8 T cells. *Nature* *576*, 465–470. <https://doi.org/10.1038/s41586-019-1836-5>.
51. Cieri, N., Camisa, B., Cocchiarella, F., Forcato, M., Oliveira, G., Provasi, E., Bondanza, A., Bordignon, C., Peccatori, J., Ciceri, F., et al. (2013). IL-7 and IL-15 instruct the generation of human memory stem T cells from naive precursors. *Blood* *121*, 573–584. <https://doi.org/10.1182/blood-2012-05-431718>.
52. Gattinoni, L., Zhong, X.-S., Palmer, D.C., Ji, Y., Hinrichs, C.S., Yu, Z., Wrzesinski, C., Boni, A., Cassard, L., Garvin, L.M., et al. (2009). Wnt signaling arrests effector T cell differentiation and generates CD8+ memory stem cells. *Nat. Med.* *15*, 808–813. <https://doi.org/10.1038/nm.1982>.
53. Rajamäki, K., Taira, A., Katainen, R., Välimäki, N., Kuosmanen, A., Plaketti, R.M., Seppälä, T.T., Ahtainen, M., Wirta, E.V., Vartiainen, E., et al. (2021). Genetic and Epigenetic Characteristics of Inflammatory Bowel Disease-Associated Colorectal Cancer. *Gastroenterology* *161*, 592–607. <https://doi.org/10.1053/j.gastro.2021.04.042>.
54. Zhou, R.W., Harpaz, N., Itzkowitz, S.H., and Parsons, R.E. (2023). Molecular mechanisms in colitis-associated colorectal cancer. *Oncogenesis* *12*, 48. <https://doi.org/10.1038/s41389-023-00492-0>.
55. Zheng, Z., Wieder, T., Mauere, B., Schäfer, L., Kesselring, R., and Braumüller, H. (2023). T Cells in Colorectal Cancer: Unravelling the Function of Different T Cell Subsets in the Tumor Microenvironment. *Int. J. Mol. Sci.* *24*, 11673.
56. Efremova, M., Rieder, D., Klepsch, V., Charoentong, P., Finotello, F., Hackl, H., Herrmann-Kleiter, N., Löwer, M., Baier, G., Krogsdam, A., and Trajanoski, Z. (2018). Targeting immune checkpoints potentiates immunoeediting and changes the dynamics of tumor evolution. *Nat. Commun.* *9*, 32. <https://doi.org/10.1038/s41467-017-02424-0>.
57. Nakajima, Y., Chamoto, K., Oura, T., and Honjo, T. (2021). Critical role of the CD44^{low}CD62L^{low} CD8⁺ T cell subset in restoring antitumor immunity in aged mice. *Proc. Natl. Acad. Sci. USA* *118*, e2103730118. <https://doi.org/10.1073/pnas.2103730118>.
58. Gros, A., Robbins, P.F., Yao, X., Li, Y.F., Turcotte, S., Tran, E., Wunderlich, J.R., Mixon, A., Farid, S., Dudley, M.E., et al. (2014). PD-1 identifies the patient-specific CD8⁺ tumor-reactive repertoire infiltrating human tumors. *J. Clin. Invest.* *124*, 2246–2259. <https://doi.org/10.1172/jci73639>.
59. Ahmadzadeh, M., Johnson, L.A., Heemskerck, B., Wunderlich, J.R., Dudley, M.E., White, D.E., and Rosenberg, S.A. (2009). Tumor antigen-specific CD8 T cells infiltrating the tumor express high levels of PD-1 and are functionally impaired. *Blood* *114*, 1537–1544. <https://doi.org/10.1182/blood-2008-12-195792>.
60. Gorman, J.V., Starbeck-Miller, G., Pham, N.L.L., Traver, G.L., Rothman, P.B., Harty, J.T., and Colgan, J.D. (2014). Tim-3 directly enhances CD8 T cell responses to acute *Listeria monocytogenes* infection. *J. Immunol.* *192*, 3133–3142. <https://doi.org/10.4049/jimmunol.1302290>.
61. Chen, S., Lee, L.-F., Fisher, T.S., Jessen, B., Elliott, M., Evering, W., Logronio, K., Tu, G.H., Tsaparikos, K., Li, X., et al. (2015). Combination of 4-1BB Agonist and PD-1 Antagonist Promotes Antitumor Effector/Memory CD8 T Cells in a Poorly Immunogenic Tumor Model. *Cancer Immunol. Res.* *3*, 149–160. <https://doi.org/10.1158/2326-6066.Cir-14-0118>.
62. Moskowitz, D.M., Zhang, D.W., Hu, B., Le Saux, S., Yanes, R.E., Ye, Z., Buenrostro, J.D., Weyand, C.M., Greenleaf, W.J., and Goronzy, J.J. (2017). Epigenomics of human CD8 T cell differentiation and aging. *Sci. Immunol.* *2*, eaag0192. <https://doi.org/10.1126/sciimmunol.aag0192>.
63. Abdelsamed, H.A., Moustaki, A., Fan, Y., Dogra, P., Ghoneim, H.E., Zeb-ley, C.C., Triplett, B.M., Sekaly, R.-P., and Youngblood, B. (2017). Human memory CD8 T cell effector potential is epigenetically preserved during in vivo homeostasis. *J. Exp. Med.* *214*, 1593–1606. <https://doi.org/10.1084/jem.20161760>.
64. Hope, J.L., Stairiker, C.J., Spantidea, P.I., Gracias, D.T., Carey, A.J., Fike, A.J., van Meurs, M., Brouwers-Haspels, I., Rijsbergen, L.C., Fraietta, J.A., et al. (2017). The Transcription Factor T-Bet Is Regulated by MicroRNA-155 in Murine Anti-Viral CD8(+) T Cells via SHIP-1. *Front. Immunol.* *8*, 1696. <https://doi.org/10.3389/fimmu.2017.01696>.
65. Ji, Y., Fioravanti, J., Zhu, W., Wang, H., Wu, T., Hu, J., Lacey, N.E., Gautam, S., Le Gall, J.B., Yang, X., et al. (2019). miR-155 harnesses Pbf19 to potentiate cancer immunotherapy through epigenetic reprogramming of CD8+ T cell fate. *Nat. Commun.* *10*, 2157. <https://doi.org/10.1038/s41467-019-09882-8>.
66. O'Connell, R.M., Chaudhuri, A.A., Rao, D.S., and Baltimore, D. (2009). Inositol phosphatase SHIP1 is a primary target of miR-155. *Proc. Natl. Acad. Sci. USA* *106*, 7113–7118. <https://doi.org/10.1073/pnas.0902636106>.
67. Gumbleton, M., Sudan, R., Fernandes, S., Engelman, R.W., Russo, C.M., Chisholm, J.D., and Kerr, W.G. (2017). Dual enhancement of T and NK cell function by pulsatile inhibition of SHIP1 improves antitumor immunity and survival. *Sci. Signal.* *10*, eaam5353. <https://doi.org/10.1126/scisignal.aam5353>.
68. Lind, E.F., Elford, A.R., and Ohashi, P.S. (2013). Micro-RNA 155 Is Required for Optimal CD8+ T Cell Responses to Acute Viral and Intracellular Bacterial Challenges. *J. Immunol.* *190*, 1210–1216. <https://doi.org/10.4049/jimmunol.1202700>.
69. Ji, Y., Wrzesinski, C., Yu, Z., Hu, J., Gautam, S., Hawk, N.V., Telford, W.G., Palmer, D.C., Franco, Z., Sukumar, M., et al. (2015). miR-155 augments CD8+ T-cell antitumor activity in lymphoreplete hosts by enhancing responsiveness to homeostatic gamma-c cytokines. *Proc. Natl. Acad. Sci. USA* *112*, 476–481. <https://doi.org/10.1073/pnas.1422916112>.
70. Tarasenko, T., Kole, H.K., Chi, A.W., Mentink-Kane, M.M., Wynn, T.A., and Bolland, S. (2007). T cell-specific deletion of the inositol phosphatase SHIP reveals its role in regulating Th1/Th2 and cytotoxic responses. *Proc. Natl. Acad. Sci. USA* *104*, 11382–11387. <https://doi.org/10.1073/pnas.0704853104>.
71. Kim, E.H., Sullivan, J.A., Plisch, E.H., Tejera, M.M., Jatzek, A., Choi, K.Y., and Suresh, M. (2012). Signal Integration by Akt Regulates CD8 T Cell Effector and Memory Differentiation. *J. Immunol.* *188*, 4305–4314. <https://doi.org/10.4049/jimmunol.1103568>.
72. Hedrick, S.M., Hess Michelini, R., Doedens, A.L., Goldrath, A.W., and Stone, E.L. (2012). FOXO transcription factors throughout T cell biology. *Nat. Rev. Immunol.* *12*, 649–661. <https://doi.org/10.1038/nri3278>.
73. Kim, C., Jin, J., Weyand, C.M., and Goronzy, J.J. (2020). The Transcription Factor TCF1 in T Cell Differentiation and Aging. *Int. J. Mol. Sci.* *21*, 6497. <https://doi.org/10.3390/ijms21186497>.
74. Michelini, R.H., Doedens, A.L., Goldrath, A.W., and Hedrick, S.M. (2013). Differentiation of CD8 memory T cells depends on Foxo1. *J. Exp. Med.* *210*, 1189–1200. <https://doi.org/10.1084/jem.20130392>.
75. Rao, R.R., Li, Q., Gubbels Bupp, M.R., and Shrikant, P.A. (2012). Transcription factor Foxo1 represses T-bet-mediated effector functions and

- promotes memory CD8(+) T cell differentiation. *Immunity* 36, 374–387. <https://doi.org/10.1016/j.immuni.2012.01.015>.
76. Fabre, S., Carrette, F., Chen, J., Lang, V., Semichon, M., Denoyelle, C., Lazar, V., Cagnard, N., Dubart-Kupperschmitt, A., Mangeney, M., et al. (2008). FOXO1 Regulates L-Selectin and a Network of Human T Cell Homing Molecules Downstream of Phosphatidylinositol 3-Kinase1. *J. Immunol.* 181, 2980–2989. <https://doi.org/10.4049/jimmunol.181.5.2980>.
 77. Kerdiles, Y.M., Beisner, D.R., Tinoco, R., Dejean, A.S., Castrillon, D.H., DePinho, R.A., and Hedrick, S.M. (2009). Foxo1 links homing and survival of naive T cells by regulating L-selectin, CCR7 and interleukin 7 receptor. *Nat. Immunol.* 10, 176–184. <https://doi.org/10.1038/ni.1689>.
 78. Doan, A., Mueller, K.P., Chen, A., Rouin, G.T., Daniel, B., Lattin, J., Chen, Y., Mozarsky, B., Markovska, M., Arias-Umana, J., et al. (2023). FOXO1 is a master regulator of CAR T memory programming. Preprint at Res. Sq. <https://doi.org/10.21203/rs.3.rs-2802998/v1>.
 79. Marchais, M., Simula, L., Phayanouvong, M., Mami-Chouaib, F., Bismuth, G., Decroocq, J., Bouscary, D., Dutrieux, J., and Mangeney, M. (2023). FOXO1 Inhibition Generates Potent Nonactivated CAR T Cells against Solid Tumors. *Cancer Immunol. Res.* 11, 1508–1523. <https://doi.org/10.1158/2326-6066.Cir-22-0533>.
 80. Delpoux, A., Lai, C.Y., Hedrick, S.M., and Doedens, A.L. (2017). FOXO1 opposition of CD8(+) T cell effector programming confers early memory properties and phenotypic diversity. *Proc. Natl. Acad. Sci. USA* 114, E8865–e8874. <https://doi.org/10.1073/pnas.1618916114>.
 81. Kim, M.V., Ouyang, W., Liao, W., Zhang, M.Q., and Li, M.O. (2013). The transcription factor Foxo1 controls central-memory CD8+ T cell responses to infection. *Immunity* 39, 286–297. <https://doi.org/10.1016/j.immuni.2013.07.013>.
 82. Tooley, K., Jerby, L., Escobar, G., Krovi, S.H., Mangani, D., Dandekar, G., Cheng, H., Madi, A., Goldschmidt, E., Lambden, C., et al. (2024). Pan-cancer mapping of single CD8+ T cell profiles reveals a TCF1: CXCR6 axis regulating CD28 co-stimulation and anti-tumor immunity. *Cell Reports Medicine* 5, 101640. <https://doi.org/10.1016/j.xcrm.2024.101640>.
 83. Hsin, J.P., Lu, Y., Loeb, G.B., Leslie, C.S., and Rudensky, A.Y. (2018). The effect of cellular context on miR-155-mediated gene regulation in four major immune cell types. *Nat. Immunol.* 19, 1137–1145. <https://doi.org/10.1038/s41590-018-0208-x>.
 84. Uhlen, M., Zhang, C., Lee, S., Sjöstedt, E., Fagerberg, L., Bidkhori, G., Benfantes, R., Arif, M., Liu, Z., Edfors, F., et al. (2017). A pathology atlas of the human cancer transcriptome. *Science* 357, eaan2507. <https://doi.org/10.1126/science.aan2507>.
 85. Pecci, F., Cantini, L., Bittoni, A., Lenci, E., Lupi, A., Crocetti, S., Giglio, E., Giampieri, R., and Berardi, R. (2021). Beyond Microsatellite Instability: Evolving Strategies Integrating Immunotherapy for Microsatellite Stable Colorectal Cancer. *Curr. Treat. Options Oncol.* 22, 69. <https://doi.org/10.1007/s11864-021-00870-z>.
 86. Pelka, K., Hofree, M., Chen, J.H., Sarkizova, S., Pirl, J.D., Jorgji, V., Bejnood, A., Dionne, D., Ge, W.H., Xu, K.H., et al. (2021). Spatially organized multicellular immune hubs in human colorectal cancer. *Cell* 184, 4734–4752.e20. <https://doi.org/10.1016/j.cell.2021.08.003>.
 87. Poynter, J.N., Siegmund, K.D., Weisenberger, D.J., Long, T.I., Thibodeau, S.N., Lindor, N., Young, J., Jenkins, M.A., Hopper, J.L., Baron, J.A., et al. (2008). Molecular Characterization of MSI-H Colorectal Cancer by MLH1 Promoter Methylation, Immunohistochemistry, and Mismatch Repair Germline Mutation Screening. *Cancer Epidemiol. Biomarkers Prev.* 17, 3208–3215. <https://doi.org/10.1158/1055-9965.Epi-08-0512>.
 88. Herman, J.G., Umar, A., Polyak, K., Graff, J.R., Ahuja, N., Issa, J.P., Markowitz, S., Willson, J.K., Hamilton, S.R., Kinzler, K.W., et al. (1998). Incidence and functional consequences of hMLH1 promoter hypermethylation in colorectal carcinoma. *Proc. Natl. Acad. Sci. USA* 95, 6870–6875. <https://doi.org/10.1073/pnas.95.12.6870>.
 89. Gattinoni, L., Speiser, D.E., Lichterfeld, M., and Bonini, C. (2017). T memory stem cells in health and disease. *Nat. Med.* 23, 18–27. <https://doi.org/10.1038/nm.4241>.
 90. Wherry, E.J., Teichgräber, V., Becker, T.C., Masopust, D., Kaech, S.M., Antia, R., von Andrian, U.H., and Ahmed, R. (2003). Lineage relationship and protective immunity of memory CD8 T cell subsets. *Nat. Immunol.* 4, 225–234. <https://doi.org/10.1038/ni889>.
 91. Steinke, F.C., Yu, S., Zhou, X., He, B., Yang, W., Zhou, B., Kawamoto, H., Zhu, J., Tan, K., and Xue, H.H. (2014). TCF-1 and LEF-1 act upstream of Th-POK to promote the CD4(+) T cell fate and interact with Runx3 to silence Cd4 in CD8(+) T cells. *Nat. Immunol.* 15, 646–656. <https://doi.org/10.1038/ni.2897>.
 92. Philip, M., Fairchild, L., Sun, L., Horste, E.L., Camara, S., Shakiba, M., Scott, A.C., Viale, A., Lauer, P., Merghoub, T., et al. (2017). Chromatin states define tumour-specific T cell dysfunction and reprogramming. *Nature* 545, 452–456. <https://doi.org/10.1038/nature22367>.
 93. Yan, Y., Cao, S., Liu, X., Harrington, S.M., Bindeman, W.E., Adjei, A.A., Jang, J.S., Jen, J., Li, Y., Chanana, P., et al. (2018). CX3CR1 identifies PD-1 therapy-responsive CD8+ T cells that withstand chemotherapy during cancer chemoimmunotherapy. *JCI Insight* 3, e97828. <https://doi.org/10.1172/jci.insight.97828>.
 94. Stelekati, E., Chen, Z., Manne, S., Kurachi, M., Ali, M.-A., Lewy, K., Cai, Z., Nzingha, K., McLane, L.M., Hope, J.L., et al. (2018). Long-Term Persistence of Exhausted CD8 T Cells in Chronic Infection Is Regulated by MicroRNA-155. *Cell Rep.* 23, 2142–2156. <https://doi.org/10.1016/j.celrep.2018.04.038>.
 95. Ahn, E., Araki, K., Hashimoto, M., Li, W., Riley, J.L., Cheung, J., Sharpe, A.H., Freeman, G.J., Irving, B.A., and Ahmed, R. (2018). Role of PD-1 during effector CD8 T cell differentiation. *Proc. Natl. Acad. Sci. USA* 115, 4749–4754. <https://doi.org/10.1073/pnas.1718217115>.
 96. Tume, P.C., Harview, C.L., Yearley, J.H., Shintaku, I.P., Taylor, E.J.M., Robert, L., Chmielowski, B., Spasic, M., Henry, G., Ciobanu, V., et al. (2014). PD-1 blockade induces responses by inhibiting adaptive immune resistance. *Nature* 515, 568–571. <https://doi.org/10.1038/nature13954>.
 97. Kim, C., Jin, J., Weyand, C.M., and Goronzy, J.J. (2020). The Transcription Factor TCF1 in T Cell Differentiation and Aging. *Int. J. Mol. Sci.* 21, 6497.
 98. Delpoux, A., Marcel, N., Hess Michelini, R., Katayama, C.D., Allison, K.A., Glass, C.K., Quiñones-Parra, S.M., Murre, C., Loh, L., Kedzierska, K., et al. (2021). FOXO1 constrains activation and regulates senescence in CD8 T cells. *Cell Rep.* 34, 108674. <https://doi.org/10.1016/j.celrep.2020.108674>.
 99. Emiloju, O.E., and Sinicrope, F.A. (2023). Neoadjuvant Immune Checkpoint Inhibitor Therapy for Localized Deficient Mismatch Repair Colorectal Cancer: A Review. *JAMA Oncol.* 9, 1708–1715. <https://doi.org/10.1001/jamaoncol.2023.3323>.
 100. Taieb, J., Srvec, M., Cohen, R., Basile, D., Tougeron, D., and Phelip, J.-M. (2022). Deficient mismatch repair/microsatellite unstable colorectal cancer: Diagnosis, prognosis and treatment. *Eur. J. Cancer* 175, 136–157. <https://doi.org/10.1016/j.ejca.2022.07.020>.
 101. Gareev, I., Beyerli, O., Yang, G., Sun, J., Pavlov, V., Izmailov, A., Shi, H., and Zhao, S. (2020). The current state of miRNAs as biomarkers and therapeutic tools. *Clin. Exp. Med.* 20, 349–359. <https://doi.org/10.1007/s10238-020-00627-2>.
 102. Hu, R., Kagele, D.A., Huffaker, T.B., Runtsch, M.C., Alexander, M., Liu, J., Bake, E., Su, W., Williams, M.A., Rao, D.S., et al. (2014). miR-155 Promotes T Follicular Helper Cell Accumulation during Chronic, Low-Grade Inflammation. *Immunity* 41, 605–619. <https://doi.org/10.1016/j.immuni.2014.09.015>.
 103. Hafemeister, C., and Satija, R. (2019). Normalization and variance stabilization of single-cell RNA-seq data using regularized negative binomial regression. *Genome Biol.* 20, 296. <https://doi.org/10.1186/s13059-019-1874-1>.

104. Heng, T.S.P., and Painter, M.W.; Immunological Genome Project Consortium (2008). The Immunological Genome Project: networks of gene expression in immune cells. *Nat. Immunol.* **9**, 1091–1094. <https://doi.org/10.1038/ni1008-1091>.
105. Ekiz, H.A., Conley, C.J., Stephens, W.Z., and O’Connell, R.M. (2020). CIPR: a web-based R/shiny app and R package to annotate cell clusters in single cell RNA sequencing experiments. *BMC Bioinf.* **21**, 191. <https://doi.org/10.1186/s12859-020-3538-2>.
106. Andreatta, M., Corria-Osorio, J., Müller, S., Cubas, R., Coukos, G., and Carmona, S.J. (2021). Interpretation of T cell states from single-cell transcriptomics data using reference atlases. *Nat. Commun.* **12**, 2965. <https://doi.org/10.1038/s41467-021-23324-4>.
107. Dong, M.B., Wang, G., Chow, R.D., Ye, L., Zhu, L., Dai, X., Park, J.J., Kim, H.R., Errami, Y., Guzman, C.D., et al. (2019). Systematic Immunotherapy Target Discovery Using Genome-Scale In Vivo CRISPR Screens in CD8 T Cells. *Cell* **178**, 1189–1204.e23. <https://doi.org/10.1016/j.cell.2019.07.044>.
108. Jaiswal, A.K., Truong, H., Tran, T.M., Lin, T.L., Casero, D., Alberti, M.O., and Rao, D.S. (2021). Focused CRISPR-Cas9 genetic screening reveals USO1 as a vulnerability in B-cell acute lymphoblastic leukemia. *Sci. Rep.* **11**, 13158. <https://doi.org/10.1038/s41598-021-92448-w>.
109. Sanjana, N.E., Shalem, O., and Zhang, F. (2014). Improved vectors and genome-wide libraries for CRISPR screening. *Nat. Methods* **11**, 783–784. <https://doi.org/10.1038/nmeth.3047>.
110. Wallace, J., Hu, R., Mosbrugger, T.L., Dahlem, T.J., Stephens, W.Z., Rao, D.S., Round, J.L., and O’Connell, R.M. (2016). Genome-Wide CRISPR-Cas9 Screen Identifies MicroRNAs That Regulate Myeloid Leukemia Cell Growth. *PLoS One* **11**, e0153689. <https://doi.org/10.1371/journal.pone.0153689>.
111. Wallace, J.A., Kagele, D.A., Eiring, A.M., Kim, C.N., Hu, R., Runtsch, M.C., Alexander, M., Huffaker, T.B., Lee, S.H., Patel, A.B., et al. (2017). miR-155 promotes FLT3-ITD-induced myeloproliferative disease through inhibition of the interferon response. *Blood* **129**, 3074–3086. <https://doi.org/10.1182/blood-2016-09-740209>.
112. Pear, W.S., Miller, J.P., Xu, L., Pui, J.C., Soffer, B., Quackenbush, R.C., Pendergast, A.M., Bronson, R., Aster, J.C., Scott, M.L., and Baltimore, D. (1998). Efficient and rapid induction of a chronic myelogenous leukemia-like myeloproliferative disease in mice receiving P210 bcr/abl-transduced bone marrow. *Blood* **92**, 3780–3792.
113. Morita, S., Kojima, T., and Kitamura, T. (2000). Plat-E: an efficient and stable system for transient packaging of retroviruses. *Gene Ther.* **7**, 1063–1066. <https://doi.org/10.1038/sj.gt.3301206>.
114. Biswas, D., Takahata, S., and Stillman, D.J. (2008). Different genetic functions for the Rpd3(L) and Rpd3(S) complexes suggest competition between NuA4 and Rpd3(S). *Mol. Cell Biol.* **28**, 4445–4458. <https://doi.org/10.1128/mcb.00164-08>.
115. Coleman, S., Xie, M., Tarhini, A.A., and Tan, A.C. (2023). Systematic evaluation of the predictive gene expression signatures of immune checkpoint inhibitors in metastatic melanoma. *Mol. Carcinog.* **62**, 77–89. <https://doi.org/10.1002/mc.23442>.
116. Ritchie, M.E., Phipson, B., Wu, D., Hu, Y., Law, C.W., Shi, W., and Smyth, G.K. (2015). limma powers differential expression analyses for RNA-sequencing and microarray studies. *Nucleic Acids Res.* **43**, e47. <https://doi.org/10.1093/nar/gkv007>.
117. Zhu, A., Ibrahim, J.G., and Love, M.I. (2019). Heavy-tailed prior distributions for sequence count data: removing the noise and preserving large differences. *Bioinformatics* **35**, 2084–2092. <https://doi.org/10.1093/bioinformatics/bty895>.

STAR★METHODS

KEY RESOURCES TABLE

REAGENT or RESOURCE	SOURCE	IDENTIFIER
Antibodies		
Brilliant Violet 605™ anti-mouse IFN- γ antibody (clone #XMG1.2)	BioLegend	Cat#505839; RRID:AB_2561438
BV785 anti-mouse CD197 (CCR7) Antibody (Clone #4B12)	BioLegend	Cat#120127; RRID:AB_2716209
PE/Dazzle™ 594 anti-mouse CD366 (Tim-3) Antibody (Clone #134013)	Cell Signaling	Cat#134014; RRID:AB_2632738
APC-Cy7 anti-mouse CD3e Antibody (Clone #17A2)	BioLegend	Cat#100222; RRID:AB_2242784
BV711 anti-mouse CD3e Antibody (Clone #145-2C11)	BioLegend	Cat#100349; RRID:AB_2565841
Pacific Blue anti-mouse CD44 Antibody (Clone #IM7)	eBioscience	Cat#103019; RRID:AB_493682
PerCp/Cy5.5 anti-mouse CD44 Antibody (Clone #IM7)	BioLegend	Cat#103032; RRID:AB_2076204
APC anti-mouse CD45 Antibody (Clone #30-F11)	BioLegend	Cat#103112; RRID:AB_312977
FITC anti-mouse CD45 Antibody (Clone #30-F11)	BioLegend	Cat#103108; RRID:AB_312973
Pacific Blue anti-mouse CD45 Antibody (Clone #30-F11)	BioLegend	Cat#103126; RRID:AB_493535
PE-Cy7 anti-mouse CD45 Antibody (Clone #30-F11)	BioLegend	Cat#103114; RRID:AB_312979
Alexa Fluor® 700 anti-mouse CD62L Antibody (Clone #MEL-14)	BioLegend	Cat#104426; RRID:AB_493719
APC anti-mouse CD62L Antibody (Clone #MEL-14)	BioLegend	Cat#104412; RRID:AB_313099
BV510 anti-mouse CD62L Antibody (Clone #MEL-14)	BioLegend	Cat#104441; RRID:AB_2561537
BV785 anti-mouse CD8a Antibody (Clone #53-6.7)	BioLegend	Cat#100749; RRID:AB_11218801
FITC anti-mouse CD8a Antibody (Clone #53-6.7)	BioLegend	Cat#100706; RRID:AB_312745
PE/Dazzle™ 594 anti-mouse CD8a Antibody (Clone #53-6.7)	BioLegend	Cat#100761; RRID:AB_2564026
PerCp-Cy5.5 anti-mouse CD8a Antibody (Clone #53-6.7)	BioLegend	Cat#100734; RRID:AB_2075238
BV605 anti-mouse Cx3cr1 Antibody (Clone #SA011F11)	BioLegend	Cat#149027; RRID:AB_2565937
PerCp-Cy5.5 anti-mouse Cxcr6 Antibody (Clone #SA051D1)	eBioscience	Cat#151121; RRID:AB_2888878
Alexa Fluor® 700 anti-mouse Gzmb Antibody (Clone #QA16A02)	BioLegend	Cat#372222; RRID:AB_2728389
FITC anti-mouse Gzmb Antibody (Clone #QA16A02)	BioLegend	Cat# 372206; RRID:AB_2687030
PE anti-mouse IFN- γ Antibody (Clone #XMG1.2)	eBioscience	Cat#12-7311-82; RRID:AB_466193
APC anti-mouse p-AKT Antibody (Clone #SDRNR)	eBioscience	Cat#17-9715-42; RRID:AB_2573310
PE-Cy7 anti-mouse PD-1 Antibody	BioLegend	Cat#109110; RRID:AB_572017
PE anti-mouse SHIP1 Antibody (Clone #P1C1-A5)	BioLegend	Cat#656603; RRID:AB_2562867
Alexa Fluor® 488 anti-mouse TCF-1 Antibody (Clone #C63D9)	Cell Signaling	Cat#6444S; RRID:AB_2797627
GhostDye780 Live/Dead Stain	Tonbo Bioscience	Cat#13-0865-T100
Anti-SHIP-1 Antibody (Clone #D1163)	Cell Signaling	Cat#2728S; RRID:AB_2126244
Anti-Gapdh Antibody (Clone #D4C6R)	Cell Signaling	Cat#97166; RRID:AB_2756824
Anti-PD-1 Antibody (Clone #RMP-1-14)	BioXCell	Cat#BE0146; RRID:AB_10949053
Phospho FoxO1 (Ser256) antibody	Cell Signaling	Cat#9461S; RRID:AB_329831
Foxo1 (D7C1H) mouse mAb	Cell Signaling	Cat#14952S; RRID:AB_2722487
PE Goat anti-mouse IgG (minimal x-reactivity) Antibody	Biolegend	Cat#405307; RRID:AB_315010
APC-AffiniPure F(ab') ₂ Fragment Donkey Anti-Rabbit IgG (H + L)	Jackson ImmunoResearch	Cat#711-136-152; RRID:AB_2340601

(Continued on next page)

REAGENT or RESOURCE	SOURCE	IDENTIFIER
Continued		
Bacterial and virus strains		
pMIG-RI OVA Vector	https://doi.org/10.1038/nature07657	
MSCV hU6-sgRNA-mCherry Vector	https://www.nature.com/articles/s41598-021-92448-w	
Ship1-CRISPR A in MgRCh Plasmid, Inpp5d Mm gRNA A_26077	O'Connell Lab	P 585
Ship1-CRISPR B in MgRCh Plasmid, Inpp5d Mm gRNA A 26079	O'Connell Lab	P 586
CTRL CRISPR Pool in MgRCh	O'Connell Lab	P 589
pNL1.1 [Nluc/PGK]	Promega	Cat#N1441
PGK-NLuc-3mer miR155 Sensor	O'Connell Lab	P 617
PGK-NLuc-Mm Tcf7 UTR	O'Connell Lab	P 619
PGK-NLuc-Mm Tcf7L2 UTR	O'Connell Lab	P 620
pLenti III EF1a GFP Mm MiR155 HG	O'Connell Lab	P 621
pGL4.13[luc2/SV40]	Promega	Cat#E6681
miR155-CRISPR A in MgRCh.	O'Connell Lab	P 633
miR155-CRISPR B in MgRCh.	O'Connell Lab	P 634
pCL-Eco CMV-MMLV Gag-Pol-Env Vector	https://doi.org/10.1128/JVI.70.8.5701-5705.1996	N/A
Biological samples		
HEK293T/17 Cell Line	ATCC	Cat#CRL-11268
PLAT-E Cell Line	Cell Biolabs	Cat#RV-101
Chemicals, peptides, and recombinant proteins		
Azoxymethane (AOM)	Sigma Aldrich	Cat#A5486
Dextran Sodium Sulfate (DSS)	MP Biomedicals	Cat#0216011080
Trypan Blue	VWR	Cat#VWRVK940
Accumax	Innovative Cell Technologies	Cat# AM105
PMA	Sigma Aldrich	Cat#P1585
Ionomycin	Sigma Aldrich	Cat#10634
GolgiPlug	BD	Cat#BDB555029
BSA	Miltenyi Biotec	Cat#130-0910376
qScript cDNA SuperMix	QuantaBio	Cat#101414-106
PowerUp SYBR Green Master Mix	Applied Biosciences	Cat#A25742
BioT	Bioland Scientific LLC	Cat#B015
Polybrene Infection/Transfection Reagent	EMD Millipore	Cat#TR1003G
RetroNectin	Takara Bio	Cat#T100B
LentiX Concentrator	Takara Bio	Cat#631232
eBioscience Fixation Buffer	eBioscience	Cat#00-8222-49
Complete EDTA-free Protease Inhibitor Cocktail	Roche	Cat#04693132001
Critical commercial assays		
RNAqueous Total RNA Isolation Kit	Ambion	Cat#AM1931
miCURY LNA miRNA PCR Assay	Qiagen	Cat#339320
CD8 ⁺ T cell Isolation Kit	Miltenyi Biotec	Cat#130-104-075
Gibco Dynabeads Mouse T cell Activator CD3/CD28 for T cell Activation and Expansion	Thermo Fisher Scientific	Cat#11452D
Foxp3/Transcription Factor Buffer Staining Kit	eBioscience	Cat#00-5523-00
Deposited data		
Broad Institute Single Cell Portal Human Colon Cancer Atlas	Broad Institute	c295

(Continued on next page)

Continued

REAGENT or RESOURCE	SOURCE	IDENTIFIER
Human Protein Atlas	The Human Protein Atlas	https://www.proteinatlas.org/ENSG00000168918-INPP5D/pathology
The Cancer Genome Atlas	NCI	https://www.cancer.gov/tcga
scRNAseq data from this work	Gene Expression Omnibus (GEO)	GSE262873
Experimental models: Cell lines		
MC-38 Cell Line	Kerafast	Cat#ENH204-FP; RRID: CVCL_B288
Experimental models: Organisms/strains		
Mouse: miR-155 TKO, C57/Bl6 miR-155 fL/fL CD4 ⁺ Cre	O'Connell Lab	https://doi.org/10.1016/j.immuni.2014.09.015
Mouse: miR-155 KO, C57/Bl6 miR-155-/-	O'Connell Lab	https://doi.org/10.1016/j.celrep.2012.10.025
Mouse: OT1-Cas9, C57BL/6-Tg(TcraTcrb)1100Mjb/J B6J.129(Cg) x <i>Gt(ROSA)26Sor^{tm1.1(CAG-cas9⁺, -EGFP)Fezh}/J</i>	O'Connell Lab	Jackson Strain #003831 x #026179
Mouse: OT1-Cas9 miR-155KO, OT1-Cas9, C57BL/6-Tg(TcraTcrb)1100Mjb/J B6J.129(Cg) x <i>Gt(ROSA)26Sor^{tm1.1(CAG-cas9⁺, -EGFP)Fezh}/J</i> x miR-155-/-	O'Connell Lab	Jackson Strain #003831 x #026179 x miR-155-/-
Mouse: Tcrβ KO, B6.129P2- <i>Tcrb^{tm1Mom}/J</i>	Jackson Labs	Jackson Strain #002118
Oligonucleotides		
Mm Rpl32 F		ATCAGGCACCAGTCAGACC
Mm Rpl32 R		TTGAACCTTCTCCGCACCC
hShip1 F1		GCGTGCTGTATCGGAATTGC
hShip1 R1		TGGTGAAGAACCTCATGGAGAC
Mm Ship1 qPCR F		aAGAAACAAGCATTCCGGAGCAGc
Mm Ship1 qPCR R		CAGAGTCGTCGCCGTGTCTTTCc
gRNA Amplicon Seq F		acactctttccctacacgacgctcttccgat ctACACAAAGATATTAGTACAA AATACGTGAC
gRNA Amplicon Seq R		gactggagttcagacgtgtgctctt ccgatctTAGCGAATTCCG GGATCCTG
U6 snRNA	Qiagen	Cat#339306
hsa-miR-155-5p	Qiagen	Cat#YP02119311
mmu-miR-155-5p	Qiagen	Cat#YP02119303
Software and algorithms		
Prism	GraphPad	N/A
FlowJo	FlowJo LLC	N/A
Cell Ranger	10xGenomics	N/A
R	CRAN	N/A
Rstudio	Posit	N/A
Seurat R Package	https://doi.org/10.1038/nbt.4096	N/A
ProjecTIL R Package	https://doi.org/10.1038/s41467-021-23324-4	N/A

EXPERIMENTAL MODEL AND STUDY PARTICIPANT DETAILS

Mice

All mice in this study were on a C57BL/6 genetic background, used between 8 and 14 weeks old, and housed in the animal facility at the University of Utah. All animal care/husbandry practices and use procedures were in compliance with and approved by the Institutional Animal Care and Use Committee (IACUC) at the University of Utah and by the Association for Assessment and Accreditation of Laboratory Animal Care (AAALAC) international.

For each experiment, mice were age and sex-matched and both sexes were incorporated into each group, as no observable sex-dependent differences were detected. The mouse strains used in this study were the following: miR-155fL/fL-CD4Cre+/-,-

OT1-Cas9, OT1-Cas9-miR-155KO, miR-155^{-/-}, and Tcr β KO. miR-155fL/fL-CD4Cre^{+/-} were generated by crossing miR-155 fL/fL and CD4Cre mice to create miR-155fL/fL-CD4Cre^{+/-}.¹⁰² OT1-Cas9 mice were generated by crossing OT-1 mice (Jackson strain #003831) and Rosa26-Cas9 knock-in mice (Jackson strain #026179). Lastly, OT1-Cas9-miR-155KO animals were generated by crossing OT1-Cas9 mice with miR-155^{-/-} mice.⁶⁶ Tcr β KO mice were purchased from The Jackson Laboratory (Strain #002118). For experiments involving CD4Cre recombinase-driven miR-155 fL/fL conditional knockout mice, littermate CD4Cre^{-/-} mice were used as wildtype controls. Mice were genotyped by PCR upon weaning and co-housed with other mice of identical genotype and sex. All Cre-recombinase drivers were maintained at heterozygous expression.

The average male mouse weight ranged between 26 and 30g, and the average female mouse weight ranged between 18 and 22g. Mice were housed in cages with no more than 5 mice and single-housed if deemed experimentally/health status necessary. The mice were fed on the Teklad Global Soy Protein-Free Extruded diet. Mice were maintained as specific pathogen-free with regular testing of sentinel cages/mice on each rack.

Tumor cell lines

The MC38 cell line was obtained from Kerfast (cat # ENH204-FP; female; RRID: CVCL_B288) and cultured in MC38 media (Dulbecco's modified MEM with 10% fetal bovine serum, 2 mM glutamine, 0.1 mM nonessential amino acids, 1 mM sodium pyruvate, 10 mM HEPES, 50 μ g/ml gentamycin sulfate and penicillin/streptomycin) at 37°C under conditions of 5% CO₂. MC38 cells were recovered from cryopreservation for all experiments and cultured for 7 to 14 days as previously described before ectopic challenge. Retroviral transduction was used to generate the MC38-Ovalbumin (Ova) expressing cell line.

METHOD DETAILS

Tumor models

For the MC38 syngeneic ectopic model, 5E5 to 1E6 MC38 or MC38-OVA cells were washed 2x with 1XDPBS before subcutaneous transplantation in 100 μ L of 1X DPBS into the left flank of mice. The mice were monitored for tumor growth by surface area caliper measurements of length and width. The mice were sacrificed on days 12–14 or if tumors ulcerated/exceeded the length of 2cm in any direction. Tumors were then excised and weighed for mass. Manual disruption between the frosted end of glass slides was performed in complete RPMI culture media prior to processing into a single cell suspension.

For our primary CRC model, we used the Azoxymethane (AOM) (Sigma-Aldrich; cat: A5486-25MG)/Dextran Sodium Sulfate (DSS) (MP Biomedicals; cat:0216011080) model of colon cancer. We intraperitoneally administered 10mg of AOM per kg of mouse mass at a concentration of 2mg/ μ L in 1X DPBS. Following the administration of AOM, we gave mice 2.5% DSS in drinking water for three cycles every two weeks. Each cycle was 5 days long, and mice were sacrificed on day 80 post-administration of AOM to assess tumor burden and immunologic composition. The colons were harvested from mice, and the colon processing procedure is as follows: all epiploic appendages were removed from the peritoneal side of the colon. The colons were then dissected lengthwise. Tumors were counted after adding 0.04% Trypan blue (VWR; cat: VWRVK940-100ML) diluted in 1X DPBS to the luminal surface of the colon. Tumor burden was assessed by surface area caliper measurements of length and width. The tumors were excised and chopped with a razor blade, digested in 2mL of 50% Accumax diluted with complete RPMI culture media for 10–25 min under normal incubation conditions prior to single cell processing.

Secondary lymphoid organs, including spleens, tumor-draining mesenteric lymph nodes (AOM/DSS), and tumor-draining inguinal lymph nodes (MC38), were collected upon sacrificing the animals and processed into a single cell suspension.

For all single-cell suspensions, tissues were mashed and filtered through a 40 μ m cell strainer. For spleen processing, an additional RBC lysis (Biolegend; cat: 420301) step per the manufacturer's recommendation was included before flow cytometric staining and analysis. All single-cell processing steps were performed on ice or at 4°C.

For cytokine analysis of tissue samples, cells were washed with complete RPMI culture media prior to plating in a tissue-culture treated 96-well plate in 250 μ L of T cell culture media with 50 ng/mL PMA (Sigma-Aldrich; cat: P1585-1MG), 500 ng/mL ionomycin (Sigma-Aldrich; cat: 10634-1MG), and 1 μ L GolgiPlug (BD; cat: BDB555029) for 5–6 h at 37°C. Cells were washed twice with FACS buffer before flow cytometric staining and analysis.

Administration of anti-PD-1

300 μ g anti-PD-1 antibody (BioXCell; Clone: RMP1-14; cat: BE0146) in 200 μ L 1X DPBS was administered intraperitoneally in MC38 tumor-challenged mice.

Single-cell RNA sequencing and sample preparation

Mice were challenged with 1E6 MC38 cells and were administered anti-PD-1 antibody on days 7 and 10. Tumor cells were pooled by sex and treatment/genotype (n = 6–8). The tumor cells were excised and processed then into a single-cell suspension prior to staining with DAPI and APC-conjugated anti-CD45, washed twice with 1X DPBS with 0.4% BSA prior (Miltenyi), and FACS sorted on the BD FACSAria Cell Sorter. Sorted cells were washed in 1X DPBS with 0.4% BSA prior to quality control, and processing for scRNAseq performed by the High-throughput Genomics Core. The scRNAseq was performed on the 10X platform and performed according to manufacturer recommendations and sequenced on the Novaseq 6000. The gene reads were processed with the 10X Genomics Cell

Ranger pipeline. Mitochondrial gene representation and the variance of unique molecular identifier (UMI) counts were regressed out prior to analysis. The Fastq files were aligned to the refdata-gex-mm10-2020-A mouse reference dataset from 10X genomics using CellRanger count version 5.0.0, and feature-barcode matrices were generated. All subsequent analyses were performed using Seurat R package (v4.2.0). Data were preprocessed to remove low-quality cells based on the following criteria: cells with less than 300 features (considered low-quality), or more than 6000 features (potentially representing duplicates), or more than 5% mitochondrial gene fraction (indicative of stressed or dying cells) were excluded from further analysis. After removing unwanted cells from the dataset, the Seurat's `sctransform` method was used to normalize and integrate datasets.¹⁰³ After integration, dimensionality reduction was performed through Principal Component Analysis (PCA) and Uniform Manifold Approximation and Projection (UMAP) with 12 principal components. Single cells were clustered based on nearest-neighbor graph construction via `FindNeighbors` and `FindClusters` Seurat functions, and 14 clusters were identified at the resolution level of 0.6. Marker genes defining each cluster were determined using Seurat's `FindAllMarkers` function with default parameters. The output of this function (i.e., differentially expressed gene information) was used to name clusters using log fold-change dot product method of CIPR with the ImmGen database as the ref.^{104,105} Additionally, annotations of T cell clusters were verified against T cell reference datasets using ProjectTil package (v3.3).¹⁰⁶ The overall cluster-level differences were visualized by calculating the proportions of each cluster in individual samples. Differential expression analyses were performed between sample groups using the `FindMarkers()` function of Seurat, where genes that are expressed in at least 10% of the analyzed cells were considered, and the minimum fold-change threshold was set to 0.1. These analyses were performed for each cluster separately or by considering all Cd3e+ Cd8a+ cells as one cluster (defined as non-zero expression of both genes). Analysis results were depicted in volcano plots and/or violin plots.

qPCR analysis of miR-155-5p and INPP5D

De-identified RNA from human colon tumors was used (generously donated by Dr. Ellen J. Beswick, Associate Professor, Internal Medicine, University of Kentucky). Tumor tissues were collected under IRB-approved protocols at the University of Utah GI Tissue Bank. The total cellular RNA was isolated with RNAqueous (Ambion) per the manufacturer's recommendations and was quantified.

For all qPCR reactions, 400 ng of RNA was used to produce cDNA with qScript cDNA SuperMix (QuantaBio; cat:101414-106) for mRNA. PowerUp SYBR Green Master Mix (Applied Biosciences) was used according to the manufacturer's recommendations. 10ng of RNA was used for miRNA reactions permiRNA LNA RT kit (Qiagen; cat: 339306) manufacturer's recommendations. All reactions were run on an Applied Biosciences QS6 Thermocycler (Thermo).

Human colon cancer scRNAseq analysis

ScRNAseq data was analyzed through the Broad Institute's Single Cell Portal, specifically the Human Colon Cancer Atlas (c295) (https://singlecell.broadinstitute.org/single_cell/study/SCP1162/human-colon-cancer-atlas-c295#study-summary). Cell cluster analysis from samples of patients with CRC was defined by the authors of the original manuscript.⁸⁶

Analysis of SHIP-1 protein expression in human patients with cancer

The proportion of patients with cancer of each type that were SHIP-1 positive (Ab Clone: HPA070455) were adapted from The Human Protein Atlas online portal under patient pathology (<https://www.proteinatlas.org/ENSG00000168918-INPP5D/pathology>).⁸⁴ Representative antibody staining of CRC samples with antibody clone HPA070455 was accessed through the protein expression navigator for patients with CRC (<https://www.proteinatlas.org/ENSG00000168918-INPP5D/pathology/colorectal+cancer#img>).

CD8 T cell antitumor miRNA CRISPR target collection

A curated collection of miRNA CRISPRs was generated from bioinformatic analysis of human cancer datasets from The Cancer Genome Atlas. Candidate miRNAs were identified based on positive correlation to CD8A in multiple datasets, including ones overlapping between COAD, SCKM, and 1/3 of TCGA projects. Glioblastoma multiform (GMB) was excluded because it lacked miRNA sequencing data. Acute myeloid leukemia (LAML) and lymphoid neoplasm diffuse large B-cell lymphoma (DLBC) were excluded due to their hematopoietic origins. miRNAs with positive and negative prognosticating power (Cox and KM analysis in SKCM-immune or CIBERSORT-CD8a-high cohort) were then included in our custom collection. Additionally, non-conserved miRNAs between mice and humans or miRNAs with fewer than 4 sgRNA targeting sequences were excluded. Protein controls involved in T cell biology¹⁰⁷ and 8 scrambled controls were also included, resulting in 192 sgRNAs. Mutation phenotypes of these selected miRNAs were simultaneously evaluated in parallel using a single targeting pool of these sgRNAs expressed from the pMSCV.hU6.stuff.v1_EFs.mCh¹⁰⁸ (p545) retrovector marked with mCherry. Oligonucleotides encoding each of four validated Crispr targeting guides¹⁰⁹ for each miRNA and controls were individually ligated into Bbs I-digested p545. The resulting 192 plasmid clones were amplified and pooled at identical concentrations for viral packaging and integrating transduction to reduce sampling bias, allowing for more complete coverage with fewer transduced cells.

Amplicon seq of integrated CRISPR library barcode sequences

Seven days status post challenging TcrBKO mice with MC38-OVA cells, we transplanted 2E5 CRISPR target collection containing CD8 T cells intravenously and collected tumors after 14 days of tumor growth. Total tumor DNA was isolated, and the abundance of stably integrated CRISPR guide vector sequences was quantified. DNA from each isolated tumor was used as a template for

8 independent aliquots of sub-saturating PCR using primers o2011-o2012, which flank sgRNA sites in the p545-based integrants. These reactions were then re-pooled to generate amplicon libraries containing HTS adapters surrounding guide sequences. Each amplicon library was subjected to HTS amplicon sequencing (AMPLICON-EZ, Azenta Life Sciences). The relative frequency of each guide in the sequencing data from endpoint tumors is modeled as inversely correlated to the corresponding miRNA's requirement for T cell persistence in the tumor and is reported as \log_2 fold change relative to the frequency in T-cells prior to transplantation.

Retroviral generation and viral transduction

To generate the retrovirus,^{110–112} we transfected HEK293T/17 (ATCC; cat: CRL-11268; female; RRID:CVCL_1926) cells through lipofection with BioT (BiolandScientific LLC; cat: B015) with packaging plasmids encoding *gag*, *pol*, *env* and plasmids of interest. PLAT-E cells (Cell Biolabs Inc; cat: RV-101; female; RRID:CVCL_B488),¹¹³ were also used and transfected with BioT and plasmids of interest. The transfected cells were cultured in HEK293T/17 medium, which was used to generate clarified viral supernatant.

CD8 T cells were infected with clarified viral supernatant with 8 μ g/mL of Polybrene Infection/Transfection Reagent (EMD Millipore; cat: TR1003G) and centrifuged at 2000rpm for 2 h at 32C in tissue culture treated 6 well plates. For MC38 cells, we repeated the viral transduction process a second time. Alternatively, CD8 T cells were also subject to transduction in non-tissue culture treated 24 well plates coated with RetroNectin (Takara Bio; cat: T100B) with LentiXConcentrator (Takara Bio; cat: 631232) concentrated viral supernatant and centrifuged at 1500g for 45 min at 4C before an overnight incubation. The CD8 T cells were subject to a second round of viral transduction and expansion prior to use. After target cell transduction, the transduced cells were FACs sorted for selection fluorophores, including GFP or mCherry, on the BD FACSAria Cell Sorter.

CD8 T cell isolation and preparation for *in vivo* and *in vitro* use

CD8 T cells were purified from splenocytes by negative selection from OT1-Cas9 or OT1-Cas9-miR-155KO mice by MACS with a CD8⁺ T cell isolation kit (Miltenyi Biotec; cat: 130-104-075) per manufacturer's recommendations. After every isolation, a small sample of CD8 T cells was stained with APC-Cy7 conjugated anti-CD3e, and BV785 conjugated anti-CD8a and checked for purity by flow cytometry on the BD LSRFortessa. The purity of the isolated CD8⁺ T cells was >90% for all experiments. Isolated CD8 T cells were subject to *in vivo* and *in vitro* experiments.

Purified CD8⁺ T cells were activated with plate-bound anti-CD3/CD28 antibody (Biolegend; cat: 100340, 102116) coated onto tissue culture treated 6 well plates with 8 μ g/mL anti-CD3/CD28 antibody in T cell media. 24 h later, activated CD8 T cells were transduced with viral supernatant. Alternatively, 1E6 CD8⁺ T cells were activated with Gibco Dynabeads Mouse T cell activator CD3/CD28 for T cell Expansion and Activation (Thermo Fisher Scientific; cat: 11452D) per manufacturer's instructions in 24 well non-tissue culture treated plates (Nunc; cat: 144530) and subject to viral transduction with LentiXConcentrator concentrated viral supernatant. Transduced mCherry⁺ CD8 T cells were washed 2 times in 1XDPBS prior to adoptively transferring 2E5 CD8 T cells intravenously into TcrBKO mice challenged with MC38-Ova cells.

For *in vitro* use, CD8 T cells were activated with plate-bound anti-CD3/CD28 antibody (coated onto tissue culture treated 6 well plates with 1 μ g/mL anti-CD3/CD28 antibody in T cell media.

Flow cytometric analysis of single cells from lymphoid organs and tumors

Single cell suspension from tumors, lymphoid organs, and *in vitro* cultures were subject to the following protocol. Single cells were stained for GhostDye780 per the manufacturer's recommendations before staining with antibodies (1:200 dilution factor) against surface antigens in FACS buffer. If no intracellular antigens were analyzed, we proceeded to fixation in eBioscienceIC Fixation Buffer (eBioscience; cat: 00-8222-49) per the manufacturer's recommendation and prepared samples for analysis on the BD LSR Fortessa.

When performing analysis on intracellular antigens, we fixed and stained for intracellular antigens (1:50 dilution factor) using the Foxp3/Transcription Factor Staining Buffer Kit (eBioscience; cat: 00-5523-00) after surface staining per the manufacturer's recommendations. The samples were then prepared for analysis on the BD LSR Fortessa.

Western blot protocol

Cells were collected by centrifugation and snap-frozen. Cell pellets were lysed in protein lysis buffer¹¹⁴ with protease inhibitors (Roche). Whole-cell protein extracts were separated via SDS-PAGE and transferred to a 0.45 μ M nitrocellulose membrane. All experimental samples and controls used for one comparative analysis were run on the same blot/gel.

Block/probe conditions

Antibody staining of Ship1 and Gapdh was performed. Primary antibody binding was detected with IRDye-700- or IRDye-800-conjugated secondary antibodies (LI-COR, Lincoln, NE, USA) using an LI-COR Odyssey Infrared Flatbed Scanner.

QUANTIFICATION AND STATISTICAL ANALYSIS

Statistics

For the analysis of the custom *in vivo* miRNA library screen, \log_2 fc was calculated based on read counts from Amplicon sequencing of PCR amplicons of the sgRNA barcode regions compared to the input sgRNA read counts of the CD8 T cells adoptively transferred

into MC-38OVA tumor-bearing mice recipients. With an $n = 4$ for log2fc for each gene, we performed the One sample t and Wilcoxon test with a hypothetical mean of 0, given that an unchanged barcode representation is a log2fc = 0. The two-way ANOVA test with multiple comparisons was used to analyze tumor growth curves. The t test with Welsh's Correction was used for comparisons between the two groups. The One-way ordinary ANOVA test with multiple comparisons of the means of each group and Brown-Forsythe and Welch ANOVA tests with multiple comparisons of means of each group were used to analyze comparisons of three or groups. Wilcoxon rank-sum test with Bonferroni correction was used to calculate the statistical significance of log2fc for gene expression from sequencing data. Computed Pearson correlation coefficients were performed and shown for correlations between two genes. T-tests with pairwise comparisons were performed for gene expression within clinical stratifiers. The Grubbs outlier test with Alpha = 0.05 or ROUT outlier test Q = 0.01% were performed to exclude outliers in our study, noted the respective figure legends. With all statistical tests * = $p > 0.05$, ** = $p > 0.01$, *** = $p > 0.001$, and **** = $p > 0.0001$.

Collection of publicly available transcriptome expression dataset and gene signature profiles related to immunotherapy response

We collected transcriptome expression datasets related to immunotherapy response across 25 public datasets (Table 1). To determine if patients responded to immunotherapy treatment, we classified patients as responders or non-responders based on Response Evaluation Criteria in Solid Tumors (RECIST) criteria. Patients recorded as complete response or partial response were classified as responders while patients recorded as stable disease or progressive disease were classified as non-responders. Gene signatures related to immunotherapy response were mainly extracted from previous work.¹¹⁵

Calculation of gene signature performance in predicting immunotherapy response

Methods to calculate the performance accuracy in predicting immunotherapy response is based on the Area Under the Receiver Operating Curve (AUROC) as previously described.¹¹⁵ In brief, to calculate the prediction accuracy of individual gene signatures across datasets, we first standardized the gene expression signatures across samples within a cohort to a Z score. We next calculated the mean Z score of a gene signature in individual patients and stratified the patients into "high" (above the mean) or "low" (below the mean) groups based on the mean of the Z score. Finally, we determined the performance of the gene signature in predicting immunotherapy response utilizing the Z score group based on AUROC values. Gene signatures perfectly predicting immunotherapy response will have an AUCROC value of 1, whereas an AUCROC score of 0.5 indicates a random classifier.

The Cancer Genome Atlas (TCGA) patient data analysis

TCGA -COAD RNAseq and miRNAseq data as well as the patient-level clinical metadata were downloaded using TCGAbiolinks R package (v2.30). Data were normalized using counts-per-million function of edgeR (v4.0.16) package and log-transformed for generating visualizations. Differential expression analyses were conducted with raw counts using DESeq2 R package. Gene set enrichment analyses (GSEA) were performed using the fgsea R package after categorizing patients into two groups based on various criteria. The expression of genes between these two groups was ranked according to the signal-to-noise ratio (original PNAS paper). In these analyses, 50 Hallmark gene sets curated in the Molecular Signatures DataBase (MSigDB) were used. Correlations between CD8A and select genes were examined in the cpm-normalized log-transformed RNAseq and miRNAseq data. Correlation analyses were performed in the whole dataset or in the data subsets with different microsatellite instability levels.

For miRNA association with CD8A, TCGA-COAD tumor samples were categorized into CD8A-high and CD8A-low subgroups at the median expression value of CD8A within the voom-normalized RNAseq data.¹¹⁶ Differential expression analysis was performed between these two subgroups using raw miRNAseq data and DESeq2 R package after removing miRNAs that were expressed in less than 10 samples. Log fold-change was shrunk using the apeglm method,¹¹⁷ and volcano plots were generated to highlight differentially expressed miRNAs.